isvr Institute of Sound and Vibration Research

Wave Propagation, Reflection and Transmission in Non-Uniform One-Dimensional Structural Waveguides

S-K. Lee, B.R. Mace and M.J. Brennan

ISVR Technical Memorandum No 928

February 2004

University of Southampton

SCIENTIFIC PUBLICATIONS BY THE ISVR

Technical Reports are published to promote timely dissemination of research results by ISVR personnel. This medium permits more detailed presentation than is usually acceptable for scientific journals. Responsibility for both the content and any opinions expressed rests entirely with the author(s).

Technical Memoranda are produced to enable the early or preliminary release of information by ISVR personnel where such release is deemed to the appropriate. Information contained in these memoranda may be incomplete, or form part of a continuing programme; this should be borne in mind when using or quoting from these documents.

Contract Reports are produced to record the results of scientific work carried out for sponsors, under contract. The ISVR treats these reports as confidential to sponsors and does not make them available for general circulation. Individual sponsors may, however, authorize subsequent release of the material.

UNIVERSITY OF SOUTHAMPTON

INSTITUTE OF SOUND AND VIBRATION RESEARCH

DYNAMICS GROUP

Wave Propagation, Reflection and Transmission in Non-Uniform One-Dimensional Structural Waveguides

by

S-K. Lee, B.R. Mace and M.J. Brennan

ISVR Technical Memorandum No: 928

February 2004

Authorised for issue by
Professor M.J. Brennan
Group Chairman

Abstract

Wave methods are developed for the motion of a one-dimensional non-uniform structure which has variable cross-sectional area, A, and the second moment of area, I, such that $A(x) \propto x^{\mu}$ and $I(x) \propto x^{\mu+2}$, where μ is real and non-negative. In particular, a rectangular structure with linearly tapered thickness and constant width satisfies the geometric conditions. Axial and bending motions of the non-uniform structures are expressed exactly in terms of waves and their asymptotic behaviour is studied. The reflection and transmission matrices for various conditions are investigated and an application to wave transmission through a connector with linearly tapered thickness is considered. The advantages of this approach are that the response can be predicted in a straightforward manner without approximation errors and with a low computational cost, irrespective of the frequency.

Content

1. INTRODUCTION

Wave methods are suitable for the analysis of the dynamic behaviour of simple structures since they do not require powerful computing resources. However, most real structures are too complicated to apply the wave approach easily. One typical case may be a structure which has non-uniform geometric shape or/and material properties. In this report, wave methods are developed for axial and bending motions of a range of one-dimensional non-uniform structures.

The oldest problem concerning a one-dimensional non-uniform structure is possibly the one in which plane waves propagate in a horn. It is well known that the governing equation can be solved easily for several specific types of horn, the so-called Salmon's family, which includes conical, exponential and catenoidal horns [1]. Nagarkar and Finch [2] studied a bell and suggested that a sinusoidal horn can also be included in the family. As a more general case, it was found that wave propagation in a horn with a polynomial variation in cross-sectional area can be solved exactly in terms of Bessel functions [3].

The results obtained for the non-uniform horns can be generally applied to axial motion of a bar and torsion of a rod since they all have same mathematical form of the governing equation. Graff [4] indicated that the axial vibration of linear, conical, exponential, and catenoidal rods can be investigated by using the results of the same horns. Kumar and Sujith [5] derived the same solutions for the axial vibration of a rod with polynomial and sinusoidal area variation and used them to obtain natural frequencies for various boundary conditions.

For a class of non-uniform Bernoulli-Euler beams, their bending motion can be exactly expressed in terms of known functions. Cranch and Adler [6] showed that the motion of a non-uniform beam of density ρ, cross-sectional area A and the second moment of area I where $\rho A(x) \propto x^m$ and $EI(x) \propto x^n$ with m and n real and non-negative, can be solved in terms of Bessel functions if $n = m+2$, $n = m+4$, $n = m+6$ and $n = \frac{m+8}{3}$. The first three conditions include rectangular beams with linear, quadratic, and cubic thickness variation and with the width varying to any power. The last condition includes a rectangular beam where $A(x) \propto x^4$ and $I(x) \propto x^4$. For this condition, the equation of motion can be transformed into that of a uniform beam as shown by Abrate [7]. It was also found that the motion of beams where $\rho A(x) \propto e^{\alpha x}$ and $EI(x) \propto e^{\alpha x}$ with α an arbitrary constant, can be expressed simply

in terms of exponential functions [6,8]. As a general case, the motion of a beam whose cross-sectional area and second moment of area vary along the beam in a polynomial manner with any two arbitrary powers of the longitudinal coordinates was described in terms of generalized hypergeometric functions by Wang [9].

These analytical solutions have been used to obtain natural frequencies for beams with various boundary conditions and intermediate constraints [10-15]. Banerjee *et al.* [16,17] obtained static/dynamic stiffnesses for axial, torsional and flexural vibrations of non-uniform beams where $A(x) \propto x^{\mu}$ and $I(x) \propto x^{\mu+2}$ with μ real and non-negative, by using the Bessel-function solutions. Eisenberger [18] derived the static/dynamic stiffness matrices for any polynomial variation of the properties along the beam as infinite power series.

In the case where an analytical solution is difficult to obtain, approximate methods can be considered. A list of the work conducted in this area can be found in [15] and [19]. In particular, the approximate methods might be useful to model the vibration of higher order non-uniform structures such as Timoshenko beams. As well as the work described in [20], Gopalakrishnan and Doyle [21] obtained axial and flexural dynamic stiffnesses of a higher order non-uniform waveguide using the displacements of the uniform deep waveguide as Ritz functions.

Wave methods are based on propagation, reflection and transmission of waves along a structure. Reference [22] contains a summary of previous work and some applications of the wave methods. Mace [23] developed a matrix formulation including nearfield wave components. Since wave methods do not lead to numerical difficulties due to ill-conditioning, they are particularly suitable in the high frequency region.

In this report, wave methods are applied to the motion of a range of one-dimensional non-uniform structures which have cross-sectional area and second moment of area such that $A(x) \propto x^{\mu}$ and $I(x) \propto x^{\mu+2}$, with μ real and non-negative. There are several typical structures that have one-dimensional motion in acoustic and vibration problems – for example, a duct or muffler with effective cross-sectional dimension much less than a wavelength, a bar undergoing axial vibration, a rod undergoing torsional vibration and a beam undergoing bending motion. In this report, the work is mainly concerned with axial motion in a bar and bending motion in a beam. The effects of shear deformation and rotary inertia in a beam are not considered and damping is not included.

In section 2, axial motion of a non-uniform bar is reviewed and it is shown that axial motion in a non-uniform bar with a polynomial variation in cross-sectional area can be

expressed in terms of Bessel functions. The solution is formulated in terms of waves and reflection, transmission and propagation matrices are defined for various conditions.

In section 3, the governing equation of bending motion of a non-uniform beam is reviewed. It is shown that bending motion in a non-uniform beam with $A(x) \propto x^{\mu}$ and $I(x) \propto x^{\mu+2}$ can be expressed in terms of Bessel functions. The solution is formulated in terms of waves and reflection, transmission and propagation matrices are defined for various conditions. Even though the work is similar to that concerning axial motion described in section 2, care should be taken because nearfield waves exist in bending motion and bending waves are dispersive.

In section 4, it was shown that the wave methods developed in sections 2 and 3 can be usefully applied to problems concerning non-uniformity. As an example, transmission through a non-uniform connector is considered. The wave methods can give exact results without approximation errors and with low computational cost, irrespective of the frequency.

In section 5, the conclusions of this report are given.

Appendix A contains a brief review of the general wave approach to the motion of a structural waveguide. Displacement and internal force matrices are introduced as suggested by Harland *et al.* [24] and propagation matrices are defined. Also, reflection and transmission matrices at boundaries and local discontinuities are defined in terms of the displacement and internal force matrices.

In appendix B, the properties of Bessel functions are summarized. The governing equations, the recurrence relations and asymptotic behaviour are reviewed.

In appendix C, two discrete wave models which are usually applied to a continuously non-uniform waveguide are introduced and errors in the application are quantitively investigated.

2. AXIAL WAVES IN A NON-UNIFORM BAR

2.1 Introduction

There are several cases where the governing equation for axial motion of a non-uniform bar can be transformed to a differential equation with a known analytical solution. Some of these were investigated in [25]. In this section, it is shown that axial motion of a non-uniform bar with a polynomial variation in cross-sectional area can also be analysed using wave methods.

In section 2.2, axial motion of a non-uniform bar is reviewed. It is shown that, if the bar has a polynomial variation in cross-sectional area, the motion can be expressed as a linear combination of Hankel functions of the first and second kind.

In section 2.3, the result of section 2.2 is reformulated in terms of waves. Propagation, displacement and internal force matrices for the non-uniform bar with the polynomial variation in cross-sectional area are derived and asymptotic behaviour of the matrices are investigated.

In section 2.4, axial wave generation in the non-uniform bar by an external force is investigated and, in section 2.5, reflection at an end of the non-uniform bar is investigated. It is shown that the non-uniformity can be expressed in terms of dynamic stiffness.

In section 2.6, reflection and transmission matrices at a discontinuity are defined. In particular, reflection and transmission at a junction between a uniform bar and a non-uniform bar are investigated in detail.

The results are subsequently used in numerical examples in section 4.

2.2 Governing equation and its solution

The axial displacement $u(x,t)$ for the free vibration of a bar at position x and time t is governed by the differential equation

$$\frac{\partial}{\partial x}\left[EA\frac{\partial u}{\partial x}\right]=\rho A\frac{\partial^2 u}{\partial t^2} \tag{2.1}$$

where EA is the axial stiffness per unit length and ρA is the mass per unit length of the bar with E being the modulus of elasticity, A the cross-sectional area and ρ the density. If the

material properties of the bar are constant but the cross-sectional area is variable, equation (2.1) reduces to

$$\frac{1}{A(x)}\frac{\partial}{\partial x}\left[A(x)\frac{\partial u}{\partial x}\right]=\frac{\rho}{E}\frac{\partial^2 u}{\partial t^2} \tag{2.2}$$

When the time dependence of the displacement $u(x,t)$ is assumed to be of the form $e^{i\omega t}$ but suppressed here for clarity, equation (2.2) can be written as

$$\frac{d^2u}{dx^2}+\frac{d\log A(x)}{dx}\frac{du}{dx}+k_l{}^2u=0 \tag{2.3}$$

where ω is angular frequency and

$$k_l=\sqrt{\frac{\rho\omega^2}{E}} \tag{2.4}$$

is the axial wavenumber.

Consider a non-uniform bar as shown in Figure 1 where $A(x)$ has a polynomial variation with x such that

$$A(x)=A_0\left(1+\frac{x}{x_0}\right)^{\mu} \tag{2.5}$$

where x_0 is the distance from a *fictitious vertex* to the section, μ is the flaring index which is a real non-negative number, and A_0 is the cross-sectional area at $x=0$. Since

$$\frac{d(\log A)}{dx}=\frac{\mu}{\xi} \tag{2.6}$$

where $\xi=x+x_0$, equation (2.3) simplifies to

$$\frac{d^2u}{d\xi^2}+\frac{\mu}{\xi}\frac{du}{d\xi}+k_l^2u=0 \tag{2.7}$$

Equation (2.7) is identical to equation (B1.12a) if

$$\nu=\frac{\mu-1}{2}. \tag{2.8}$$

Accordingly, the displacement is given by

$$u(x)=(x+x_0)^{-\nu}\left\{C_1H_\nu^{(2)}(k_lx+k_lx_0)+C_2H_\nu^{(1)}(k_lx+k_lx_0)\right\} \tag{2.9}$$

where C_1 and C_2 are arbitrary constants and $H_\nu^{(1,2)}$ are Hankel functions of the first and second kinds, respectively. Also, the internal force $P=-EA\dfrac{\partial u}{\partial x}$ with compression being defined as positive is given by

$$P(x)=EAk_l\left(x+x_0\right)^{-\nu}\left\{C_1H_{\nu+1}^{(2)}(k_lx+k_lx_0)+C_2H_{\nu+1}^{(1)}(k_lx+k_lx_0)\right\} \tag{2.10}$$

Many different bar geometries exist which satisfy equation (2.5). One of these is a rectangular bar which has constant width b but variable thickness h such that

$$b(x)=b_0, \qquad h(x)=h_0\left(1+\alpha x\right)^{\mu} \tag{2.11a, b}$$

where b_0, h_0 and α are constants which satisfy $A_0=b_0h_0$ and $x_0=\dfrac{1}{\alpha}$. A rectangular bar which has width b and thickness h such that

$$b(x)=b_0\left(1+\alpha x\right)^{\frac{\mu}{2}}, \qquad h(x)=h_0\left(1+\alpha x\right)^{\frac{\mu}{2}} \tag{2.12a, b}$$

also satisfies equation (2.5).

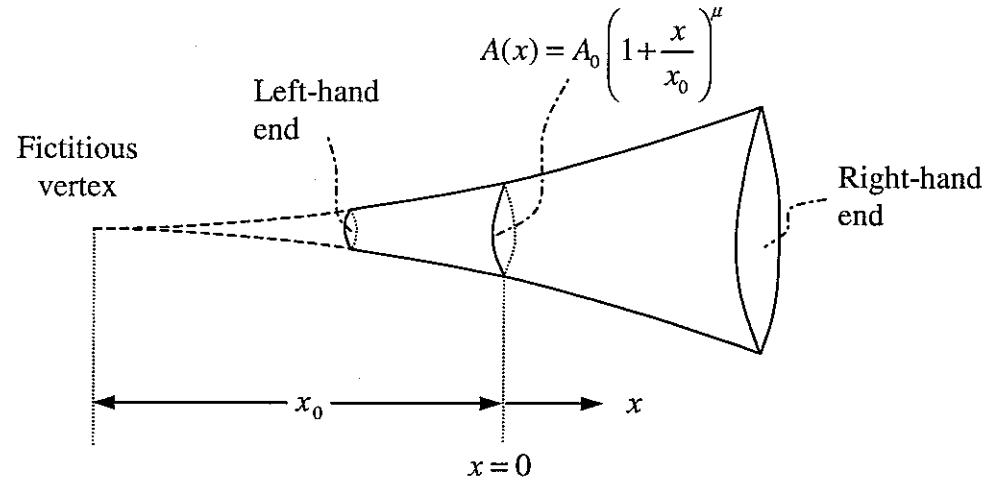

Figure 1. Non-uniform bar with polynomial variation in cross-sectional area.

2.3 The wave description

Equations (2.9) and (2.10) can be described using the wave formulation which is introduced in Appendix A.1. The displacement and internal force vectors at a section of the bar can be written as

$$\mathbf{w} = \{u\} = \Psi^{+}\mathbf{a}^{+} + \Psi^{-}\mathbf{a}^{-} \tag{2.13}$$

$$\mathbf{f} = \{P\} = \Phi^{+}\mathbf{a}^{+} + \Phi^{-}\mathbf{a}^{-} \tag{2.14}$$

where

$$\mathbf{a}^{+} = \{a^{+}\}, \qquad \mathbf{a}^{-} = \{a^{-}\} \tag{2.15a,b}$$

$$\Psi^{+} = [1], \qquad \Psi^{-} = [1] \tag{2.16a,b}$$

$$\Phi^{+} = \left[EA_0 k_l \frac{H_{\nu+1}^{(2)}(k_l x_0)}{H_{\nu}^{(2)}(k_l x_0)} \right], \qquad \Phi^{-} = \left[EA_0 k_l \frac{H_{\nu+1}^{(1)}(k_l x_0)}{H_{\nu}^{(1)}(k_l x_0)} \right] \tag{2.17a,b}$$

with

$$\nu = \frac{\mu - 1}{2} \tag{2.18}$$

The propagation matrices are then given by

$$\mathbf{F}^{+}(x) = \left[\left(\frac{x_0}{x + x_0} \right)^{\nu} \frac{H_{\nu}^{(2)}(k_l x + k_l x_0)}{H_{\nu}^{(2)}(k_l x_0)} \right], \quad \mathbf{F}^{-}(x) = \left[\left(\frac{x_0}{x + x_0} \right)^{\nu} \frac{H_{\nu}^{(1)}(k_l x + k_l x_0)}{H_{\nu}^{(1)}(k_l x_0)} \right] \tag{2.19a,b}$$

It should be noted that the propagation matrices are defined to be unit matrices at $x = 0$ and that the vectors and matrices in equations (2.13) to (2.19) are 1×1 vectors and matrices, respectively.

When $k_l x_0 \gg 1$, by using equation (B.57), the internal force matrices asymptote to those of a uniform waveguide such that

$$\Phi^{+} \approx [\mathrm{i} EA_0 k_l], \qquad \Phi^{-} \approx [-\mathrm{i} EA_0 k_l] \tag{2.20a,b}$$

Also, if the propagation length x is L, by using equation (B.56), the positive-going propagation matrix from $x = 0$ to $x = L$ and the negative-going propagation matrix from $x = L$ to $x = 0$ asymptote to

$$\mathbf{F}^{+} \approx \left[\left(\frac{x_0}{L + x_0} \right)^{\nu + \frac{1}{2}} e^{-\mathrm{i} k_l L} \right], \quad \mathbf{F}^{-} \approx \left[\left(\frac{L + x_0}{x_0} \right)^{\nu + \frac{1}{2}} e^{\mathrm{i} k_l L} \right] \tag{2.21a,b}$$

Furthermore, they asymptote to those of a uniform waveguide when the non-uniformity of the waveguide is very small, i.e., $x_0 \gg L$. Equation (2.21) implies that waves can propagate with negligible reflection as in an exponential horn.

Specifically, for a non-uniform bar with cross-sectional area satisfying equation (2.5) and $\mu = 2$,

$$\Phi^{+} = \left[EA_0 k_l \frac{H_{3/2}^{(2)}(k_l x_0)}{H_{1/2}^{(2)}(k_l x_0)} \right] = \left[\left(\mathrm{i} + \frac{1}{k_l x_0} \right) EA_0 k_l \right] \tag{2.22}$$

$$\mathbf{F}^{+}(x) = \left[\left(\frac{x_0}{x + x_0} \right)^{\frac{1}{2}} \frac{H_{1/2}^{(2)}(k_l x + k_l x_0)}{H_{1/2}^{(2)}(k_l x_0)} \right] = \left[\frac{x_0}{x + x_0} e^{-\mathrm{i}k_l x} \right] \tag{2.23}$$

It can be seen that the internal force matrix has the additional term $\frac{EA_0}{x_0}$, compared to that of the uniform bar.

2.4 Wave generation by local excitation

Consider a non-uniform bar with variable cross-sectional area satisfying equation (2.5). If the left-hand end of the bar is excited by a harmonic force $F_{ext} e^{\mathrm{i}\omega t}$ as shown in Figure 2, then a positive-going wave will be generated by the force. Since equilibrium condition at the end is given by

$$P(0) = F_{ext}; \qquad EA_0 \left[\frac{H_{\nu+1}^{(2)}(k_l x_0)}{H_{\nu}^{(2)}(k_l x_0)} k_l \right] \mathbf{q}^{+} = F_{ext} \tag{2.24}$$

then amplitude vector of the wave induced by the external force, $\mathbf{q}^{+}$, is given by

$$\mathbf{q}^{+} = \left\{ \frac{H_{\nu}^{(2)}(k_l x_0)}{H_{\nu+1}^{(2)}(k_l x_0)} \frac{F_{ext}}{EA_0 k_l} \right\} \tag{2.25}$$

Specifically, when $\mu = 0$, $\mathbf{q}^{+}$ is given by

$$\mathbf{q}^{+} = \left\{ \frac{H_{-1/2}^{(2)}(k_l x_0)}{H_{1/2}^{(2)}(k_l x_0)} \frac{F_{ext}}{EA_0 k_l} \right\} = \left\{ \frac{F_{ext}}{\mathrm{i}EA_0 k_l} \right\} \tag{2.26}$$

which is identical to that of a uniform bar and, when $\mu = 2$, $\mathbf{q}^{+}$ is given by

$$\mathbf{q}^{+} = \left\{ \frac{H_{1/2}^{(2)}(k_l x_0)}{H_{3/2}^{(2)}(k_l x_0)} \frac{F_{ext}}{EA_0 k_l} \right\} = \left\{ \frac{1}{1 + \frac{1}{\mathrm{i}k_l x_0}} \frac{F_{ext}}{\mathrm{i}EA_0 k_l} \right\} = \left\{ \frac{F_{ext}}{\mathrm{i}EA_0 k_l + \frac{EA_0}{x_0}} \right\} \tag{2.27}$$

In equation (2.27), it can be seen that the non-uniformity of the bar introduces the additional dynamic stiffness term. This term makes the amplitude of the induced wave smaller than that in a uniform bar and the phase lag behind the external force by $\left(\frac{\pi}{2}-\frac{1}{k_l x_0}\right)$.

Similarly, when the right-hand end of the non-uniform bar with $\mu=2$ is excited as shown in Figure 3, $\mathbf{q}^-$ is given by

$$\mathbf{q}^- = \left\{ \frac{F_{ext}}{\mathrm{i}EA_0 k_l - \frac{EA_0}{x_0}} \right\} \tag{2.28}$$

Compared to equation (2.27), it can be seen that the sign of the additional dynamic stiffness term has changed. This sign conversion can be understood by introducing an additional mass M_{eq}, defined by

$$M_{eq} = \frac{EA_0}{x_0\omega^2} = \frac{\rho A_0}{x_0 k_l^2} \tag{2.29}$$

Then equation (2.28) is written as

$$\mathbf{q}^- = \left\{ \frac{F_{ext}}{\mathrm{i}EA_0 k_l - M_{eq}\omega^2} \right\} \tag{2.30}$$

Thus the non-uniform beam behaves like a uniform beam with an additional stiffness when the right-hand end is excited while it behaves like a uniform beam with an additional mass when the left-hand end is excited. Even though the negative sign of an additional stiffness is not usual, the notation as in equation (2.28) will be kept for simplicity in this report.

Figure 5 shows wave generation in a non-uniform bar with geometry satisfying equation (2.12) and $\mu=2$. It can be seen that, in the high frequency region, the amplitude and the phase of the induced wave in the non-uniform bar asymptote to those in the uniform bar. It can also be seen that, when the excitation point changes from the left- to the right-hand end, the amplitudes of the induced wave are the same but the phase changes symmetrically about $-\frac{\pi}{2}$.

When $\mu=1$, $\mathbf{q}^+$ is given by

$$\mathbf{q}^+ = \left\{ \frac{H_0^{(2)}(k_l x_0)}{H_1^{(2)}(k_l x_0)} \frac{F_{ext}}{EA_0 k_l} \right\} \tag{2.31}$$

which cannot be expressed in a simple form. Figure 6 shows wave generation in a non-uniform bar with geometry satisfying equation (2.11) and $\mu = 1$. Compared to Figure 5, it can be seen that the trends are same but the effect of the non-uniformity is less than that in the non-uniform bar with $\mu = 2$.

If a section of a non-uniform bar with variable cross-sectional area given by equation (2.5) is excited by a harmonic force $F_{ext}e^{i\omega t}$ as shown in Figure 4, then positive- and negative-going waves will be generated by the force. From continuity and equilibrium conditions,

$$\mathbf{q}^{+} = \mathbf{q}^{-} \tag{2.32}$$

and

$$\mathbf{q}^{+} = \left\{ \frac{F_{ext}}{EA_0 k_l} \left[\frac{H_{\nu+1}^{(2)}(k_l x_0)}{H_{\nu}^{(2)}(k_l x_0)} - \frac{H_{\nu+1}^{(1)}(k_l x_0)}{H_{\nu}^{(1)}(k_l x_0)} \right]^{-1} \right\} \tag{2.33}$$

Thus, when $\mu = 2$, $\mathbf{q}^{+}$ and $\mathbf{q}^{-}$ are given by

$$\mathbf{q}^{+} = \mathbf{q}^{-} = \left\{ \frac{F_{ext}}{\mathrm{i}2EA_0 k_l} \right\} \tag{2.34a, b}$$

which are identical to those of a uniform bar. It can be seen that there is no influence of the non-uniformity. Figure 7 shows wave generation in a non-uniform bar with geometry satisfying equation (2.12) and $\mu = 2$ and a non-uniform bar with geometry satisfying equation (2.11) and $\mu = 1$, respectively. It can be seen that the non-uniformity does not affect the amplitude when $\mu = 2$ but it does when $\mu = 1$. The phases of the induced waves in both cases are equal to $-\frac{\pi}{2}$ and are independent of frequency.

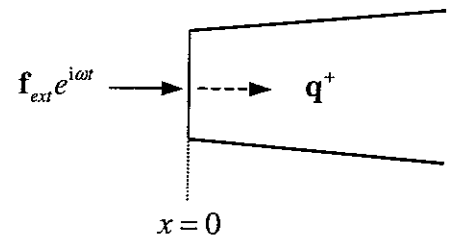

Figure 2. Non-uniform bar, left-hand side end of which is excited by local force.

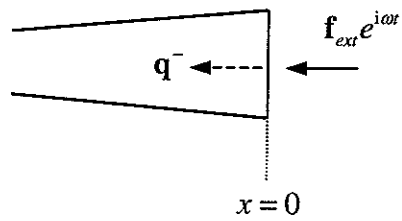

Figure 3. Non-uniform bar, right-hand side end of which is excited by local force.

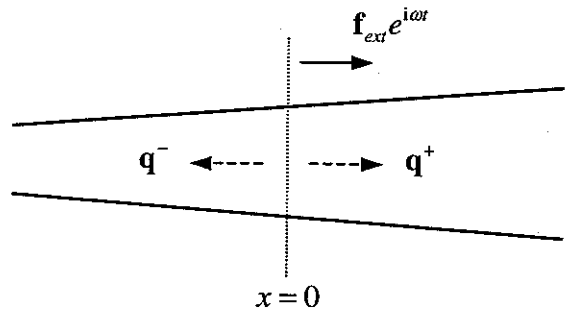

Figure 4. Non-uniform bar, a section of which is excited by local force.

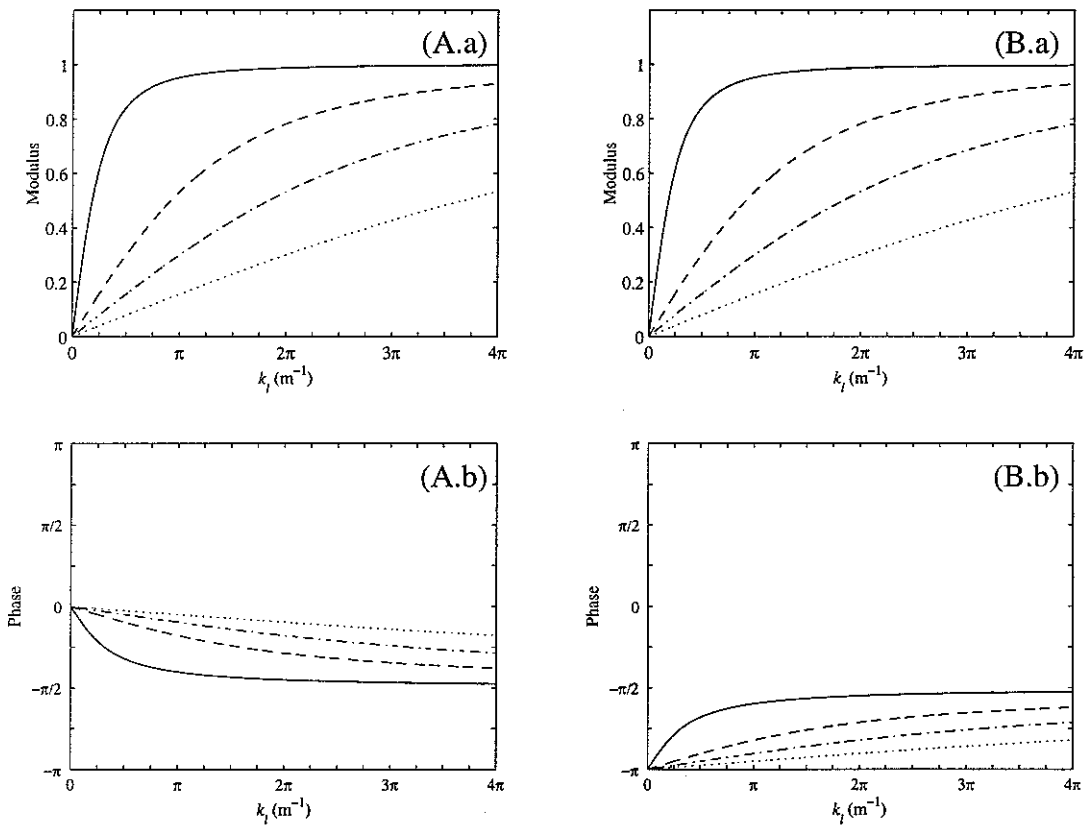

Figure 5. Axial wave generation in a non-uniform bar with geometry satisfying equation (2.12) and $\mu = 2$: (A) the left- and (B) the right-hand end is excited; (a) ratio of the amplitude of the induced wave to that in a uniform bar, (b) the phase of the induced wave;

——— , $\alpha = 1$; ------ , $\alpha = 5$; -·-·-· , $\alpha = 10$; ····· , $\alpha = 20$.

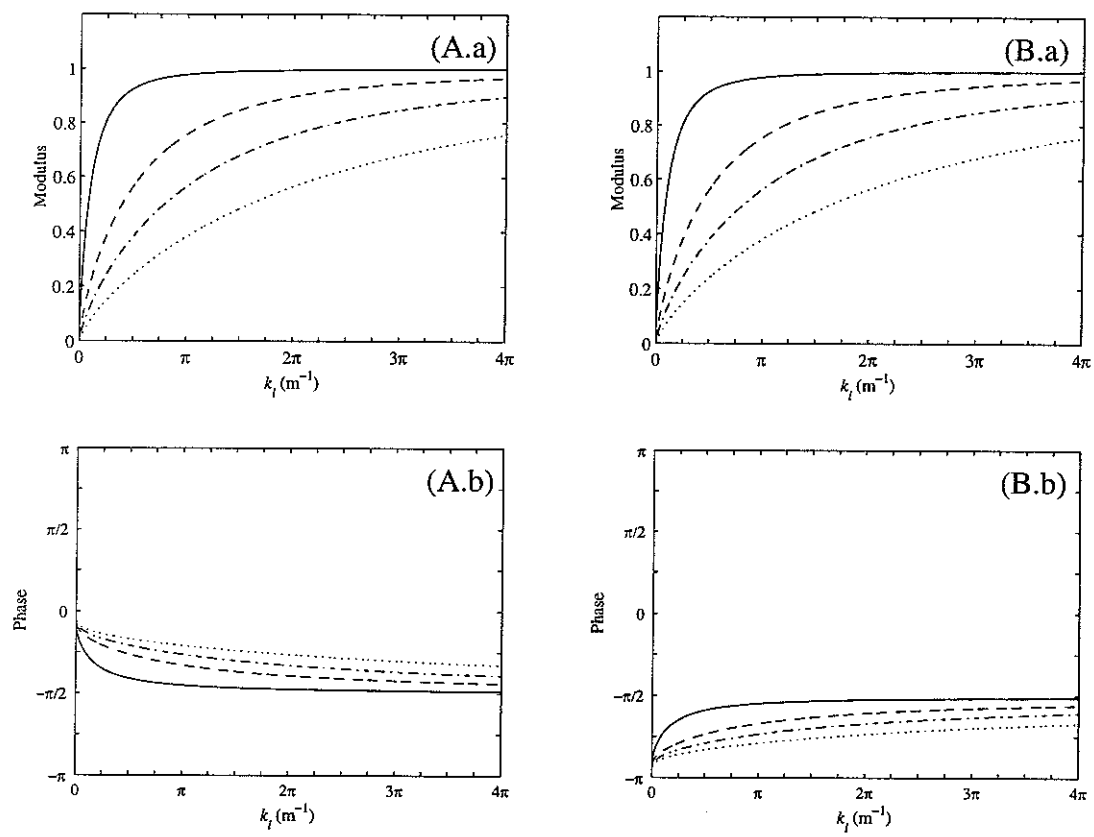

Figure 6. Axial wave generation in a non-uniform bar with geometry satisfying equation (2.11) and $\mu = 1$: (A) the left- and (B) the right-hand end is excited; (a) ratio of the amplitude of the induced wave to that in a uniform bar, (b) the phase of the induced wave;

——— , $\alpha = 1$; ------ , $\alpha = 5$; - - - - - - , $\alpha = 10$; ..... , $\alpha = 20$.

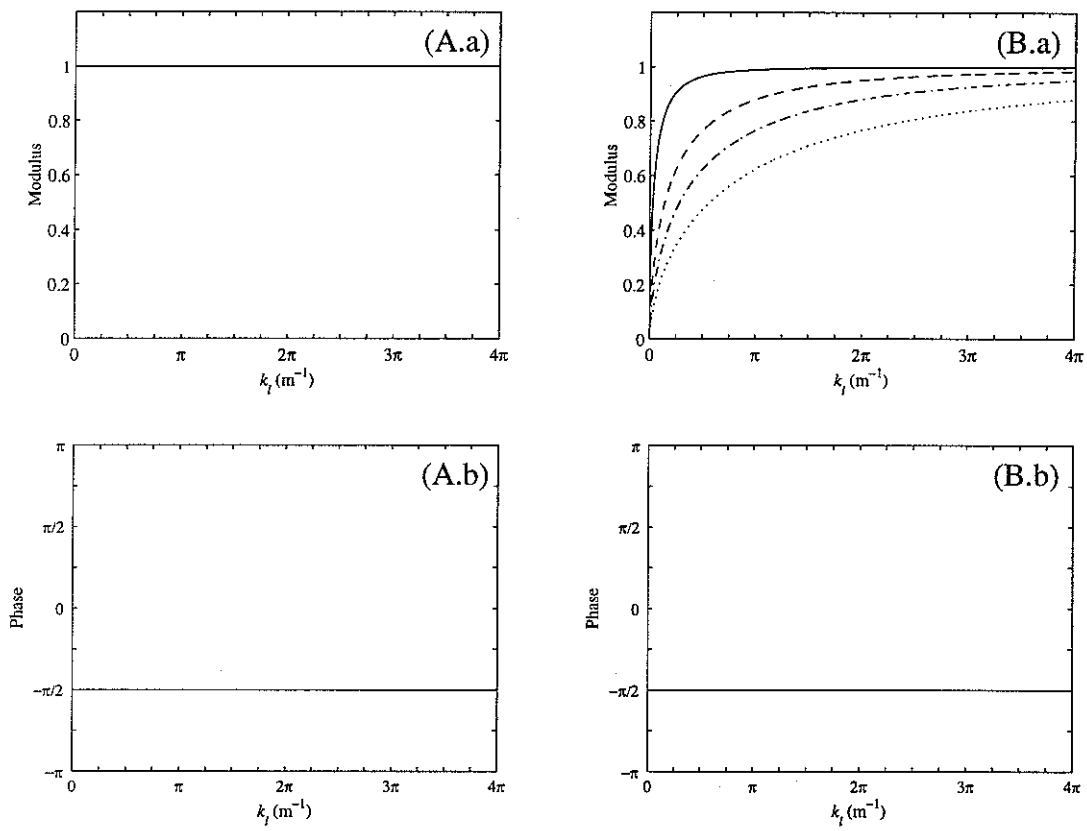

Figure 7. Axial wave generation in a non-uniform bar, at a section of which is excited by a force: the geometry of the bar satisfies (A) equation (2.12) and $\mu = 2$ and (B) equation (2.11) and $\mu = 1$; (a) ratio of the amplitude of the induced wave to that in a uniform bar, (b) the phase of the induced wave;

——— , $\alpha = 1$; ------ , $\alpha = 5$; -·-·-·- , $\alpha = 10$; ····· , $\alpha = 20$.

2.5 Reflection at a boundary

The reflection matrix **R** at the right-hand end of a waveguide is generally given by equation (A.20). If equations (A.20), (2.16) and (2.17) are combined, the reflection matrix **R** at the right-hand end of a non-uniform bar with variable cross-sectional area satisfying equation (2.5), as shown in Figure 8, is given by

$$\mathbf{R}=\left[-\frac{K_T-\dfrac{H_{\nu+1}^{(2)}(k_l x_0)}{H_\nu^{(2)}(k_l x_0)}}{K_T-\dfrac{H_{\nu+1}^{(1)}(k_l x_0)}{H_\nu^{(1)}(k_l x_0)}}\right] \tag{2.35}$$

where the dimensionless dynamic stiffness $K_T=\bar{K}_T/EA_0k_l$.

Specifically, when $\mu=2$ ($\nu=\frac{1}{2}$), **R** is given by

$$\mathbf{R}=\left[\frac{1+\mathrm{i}\left(K_T-\dfrac{1}{k_l x_0}\right)}{1-\mathrm{i}\left(K_T-\dfrac{1}{k_l x_0}\right)}\right] \tag{2.36}$$

It can be seen in equation (2.36) that the non-uniformity of the bar introduces additional dynamic stiffness. It should be noted that the reflection matrix at the left-hand end of the bar is given by equation (2.36) but with the sign of the additional stiffness term changed. When $x_0=\infty$, which means a uniform bar, equation (2.36) becomes identical to equation (2.31) in [24]. When $K_T=0$, which means a free boundary condition, the reflection matrix is given by

$$\mathbf{R}_f=-\left[\frac{1+\mathrm{i}k_l x_0}{1-\mathrm{i}k_l x_0}\right] \tag{2.37}$$

When $K_T=\infty$, i.e., a clamped boundary condition, the reflection matrix is given by

$$\mathbf{R}_c=-1 \tag{2.38}$$

It can be seen that the non-uniformity of a bar with a clamped end has no effect on the reflection matrix.

Figure 10 shows the phase of the reflection coefficient for a free boundary of a non-uniform bar with geometry satisfying equation (2.11) and $\mu=1$. It can be seen that the phase tends to zero in high frequency region. It can also be seen that the phase for the left-hand case is the opposite of that for the right-hand case.

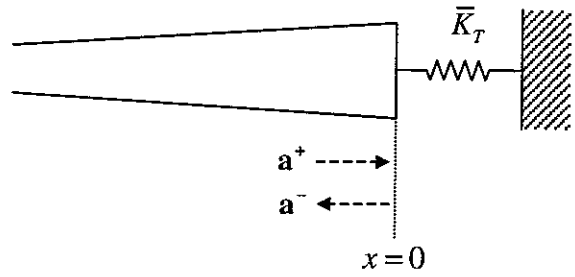

Figure 8. Right-hand boundary of a non-uniform bar.

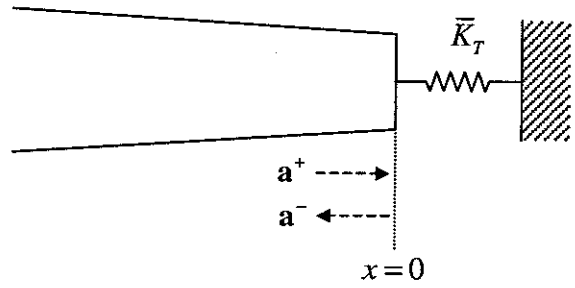

Figure 9. Left-hand boundary of a non-uniform bar.

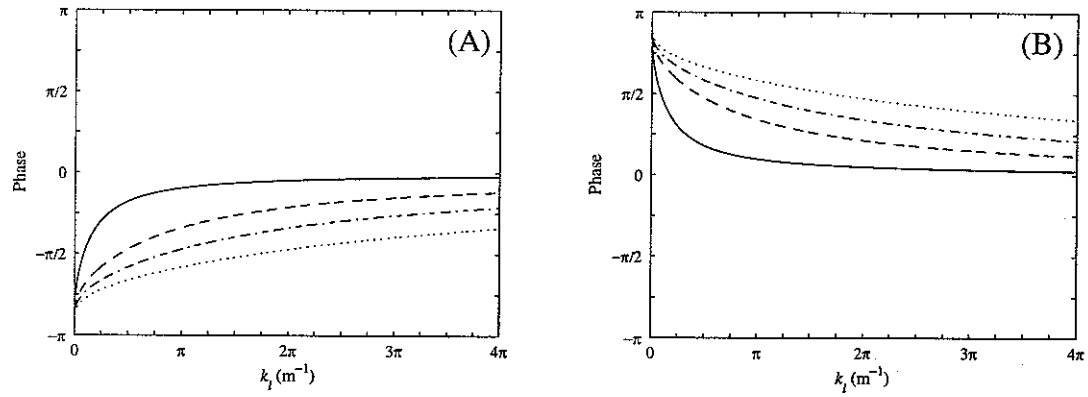

Figure 10. Phase of reflection coefficient for a free boundary of a non-uniform bar with geometry satisfying equation (2.11) and $\mu=1$: at (A) the right- and (B) the left-hand end; ——— , $\alpha=1$; ------ , $\alpha=5$; ------ , $\alpha=10$; ..... , $\alpha=20$.

2.6 Reflection and transmission at a discontinuity

The reflection matrix **R** and the transmission matrix **T** at a discontinuity in a waveguide are generally given by equations (A.29) and (A.30), respectively. If equations (A.29), (A.30), (2.16) and (2.17) are combined, **R** and **T** for the junction of two non-uniform bars with variable cross-sectional areas satisfying equation (2.5), respectively, as shown in Figure 11 are given by

$$\mathbf{R} = -\frac{\dfrac{A_{0,b}}{A_{0,a}}\dfrac{H^{(2)}_{\nu_b+1}(k_l x_{0,b})}{H^{(2)}_{\nu_b}(k_l x_{0,b})} - \dfrac{H^{(2)}_{\nu_a+1}(k_l x_{0,a})}{H^{(2)}_{\nu_a}(k_l x_{0,a})}}{\dfrac{A_{0,b}}{A_{0,a}}\dfrac{H^{(2)}_{\nu_b+1}(k_l x_{0,b})}{H^{(2)}_{\nu_b}(k_l x_{0,b})} - \dfrac{H^{(1)}_{\nu_a+1}(k_l x_{0,a})}{H^{(1)}_{\nu_a}(k_l x_{0,a})}} \tag{2.39}$$

$$\mathbf{T} = \frac{-\dfrac{H^{(1)}_{\nu_a+1}(k_l x_{0,a})}{H^{(1)}_{\nu_a}(k_l x_{0,a})} + \dfrac{H^{(2)}_{\nu_a+1}(k_l x_{0,a})}{H^{(2)}_{\nu_a}(k_l x_{0,a})}}{-\dfrac{H^{(1)}_{\nu_a+1}(k_l x_{0,a})}{H^{(1)}_{\nu_a}(k_l x_{0,a})} + \dfrac{A_{0,b}}{A_{0,a}}\dfrac{H^{(2)}_{\nu_b+1}(k_l x_{0,b})}{H^{(2)}_{\nu_b}(k_l x_{0,b})}} \tag{2.40}$$

where subscripts a and b are used to denote bars A and B, respectively.

When the cross-sectional areas of the two bars at the junction are equal, $A_{0,a} = A_{0,b}$, and the flaring indexes are given by $\mu_a = \mu_b = 2$, **R** and **T** are given by

$$\mathbf{R} = \frac{\mathrm{i}K_n}{1-\mathrm{i}K_n} \tag{2.41}$$

$$\mathbf{T} = \frac{1}{1-\mathrm{i}K_n} \tag{2.42}$$

where

$$K_n = \frac{1}{2}\left(\frac{1}{k_l x_{0,b}} - \frac{1}{k_l x_{0,a}}\right) \tag{2.43}$$

Equation (2.43) shows that the dynamic stiffness at the junction is equal to average of individual dynamic stiffnesses of the two bars. Furthermore, if the two bars have geometries satisfying equation (2.12), the dynamic stiffness can be expressed in terms of the difference of the taper rates of the two bars such that

$$K_n = \frac{1}{2}\left(\frac{\alpha_b - \alpha_a}{k_l}\right) \tag{2.44}$$

When the left-hand bar is uniform, **R** and **T** are identical to equations (2.41) and (2.42) but, here, the dimensionless dynamic stiffness K_n due to the non-uniformity is given by

$$K_n = \frac{1}{2k_l x_{0,b}} \tag{2.45}$$

Also, when the right-hand bar is uniform, **R** and **T** are identical to equations (2.41) and (2.42) but, here, the dimensionless dynamic stiffness K_n due to non-uniformity is given by

$$K_n = -\frac{1}{2k_l x_{0,a}} \tag{2.46}$$

Figure 12 shows three connection types between a uniform bar and a non-uniform bar, the cross-sectional areas of which are equal at the connection, $A_{0,a} = A_{0,b}$. It should be noticed that the type-A and type-B connections are symmetric about $x = 0$.

Figure 13 shows the power reflection and transmission coefficients for the junction of rectangular uniform and non-uniform bars, in which the non-uniform bar has variable cross-sectional area satisfying equation (2.12) when $\mu = 2$ and satisfying equation (2.11) when $\mu = 1$, respectively. The connection can be any one of the three connection types shown in Figure 12. From reciprocity, it can be noticed that the power reflection and transmission coefficients of the type-A are identical to those of the type-B. It can also be shown that the power reflection and transmission coefficients of the type-C are identical to those of the other types.

Figure 14 shows the phases of the reflection and transmission coefficients of the three connection types between a uniform bar and a non-uniform bar with cross-sectional area satisfying equation (2.12) and $\mu = 2$. It can be seen that the phases of the type-A and type-B connections are the same as each other but those of the type-C are opposite. Figure 15 shows results when the non-uniform bar has cross-sectional area satisfying equation (2.11) and $\mu = 1$. It can be seen that the trends are same as Figure 14 except that the phase of the reflection coefficient of the type-A connection shown in Figure 15-(A.a) is slightly different to that of the type-B shown in Figure 15-(B.a).

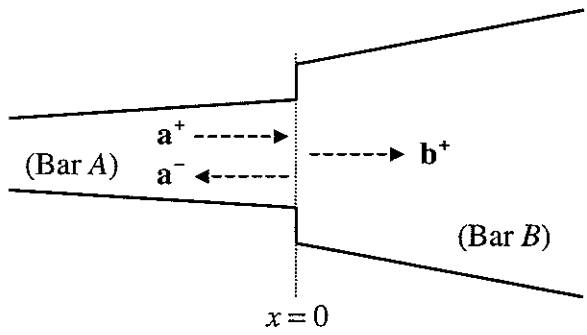

Figure 11. Connection of two non-uniform bars with different geometry.

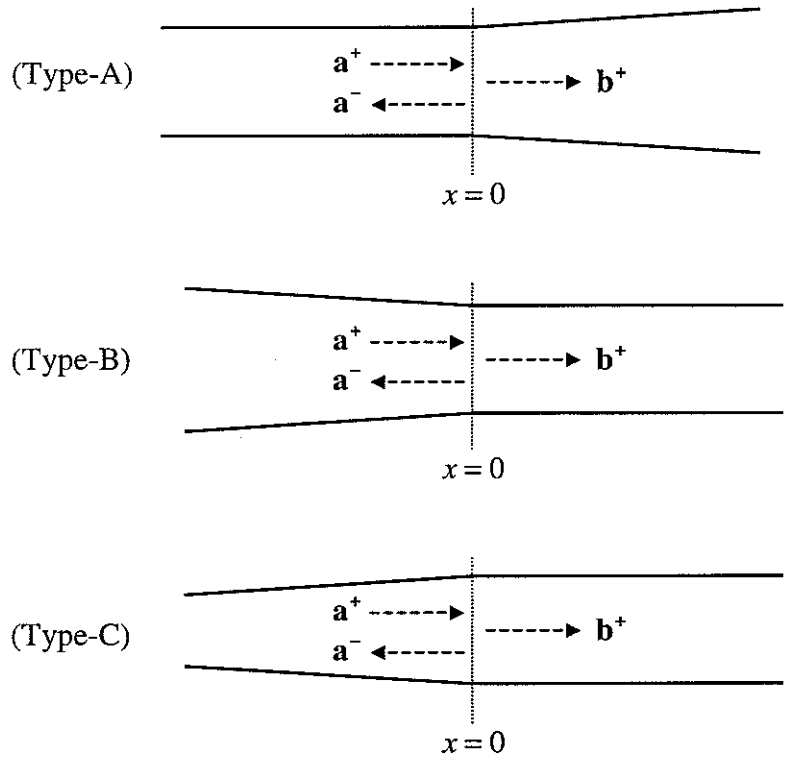

Figure 12. Three connection types between a uniform bar and a non-uniform bar.

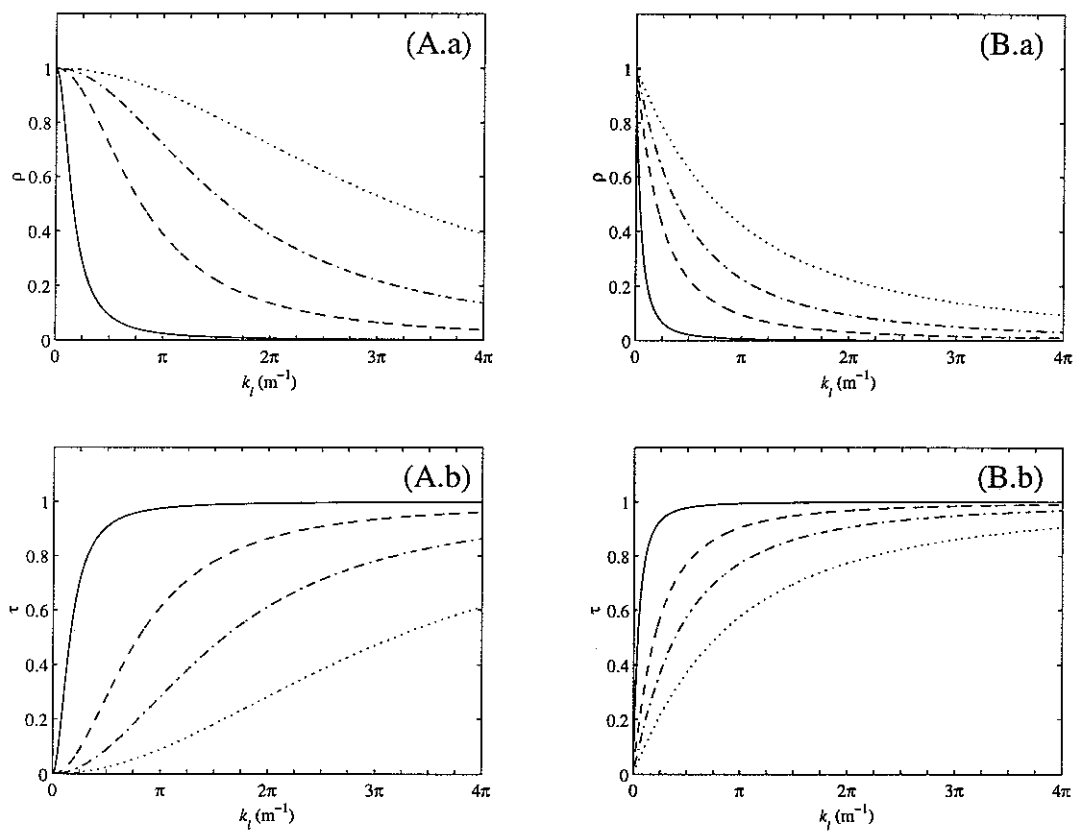

Figure 13. Power reflection and transmission coefficients for the junction of a uniform bar and a non-uniform bar: the cross-sectional area of the non-uniform bar satisfies (A) equation (2.12) and $\mu = 2$ and (B) equation (2.11) and $\mu = 1$; (a) power reflection coefficient, (b) power transmission coefficient;

——— , $\alpha = 1$; ------ , $\alpha = 5$; -·-·-·- , $\alpha = 10$; ····· , $\alpha = 20$.

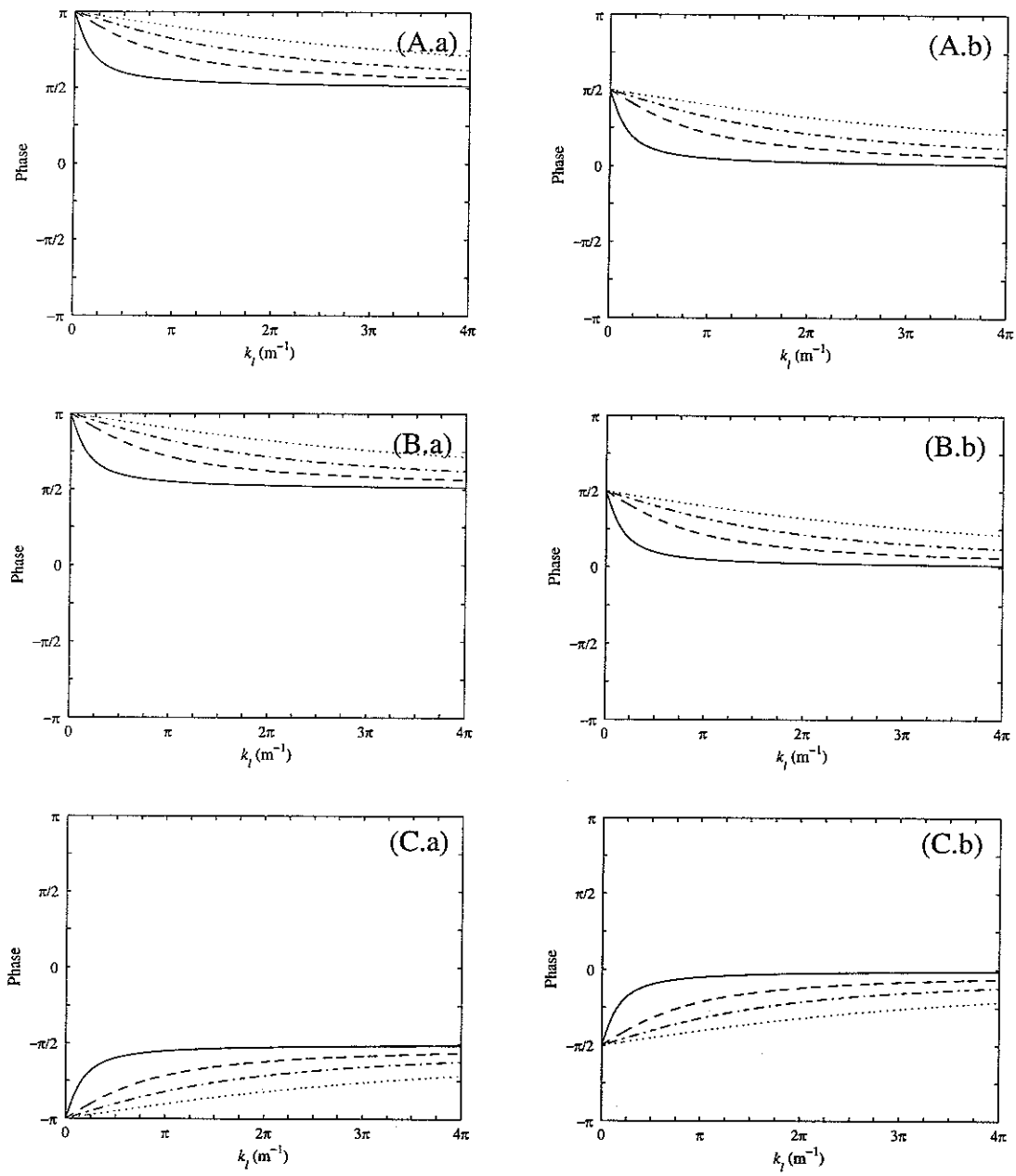

Figure 14. Phases of reflection and transmission coefficients for the junction of a uniform bar and a non-uniform bar with cross-sectional area satisfying equation (2.12) and $\mu = 2$: the connection is (A) the type-A, (B) the type-B, and (C) the type-C in Figure 12; (a) phase of reflection coefficient, (b) phase of transmission coefficient;

——— , $\alpha = 1$; ------ , $\alpha = 5$; -·-·-·- , $\alpha = 10$; ····· , $\alpha = 20$.

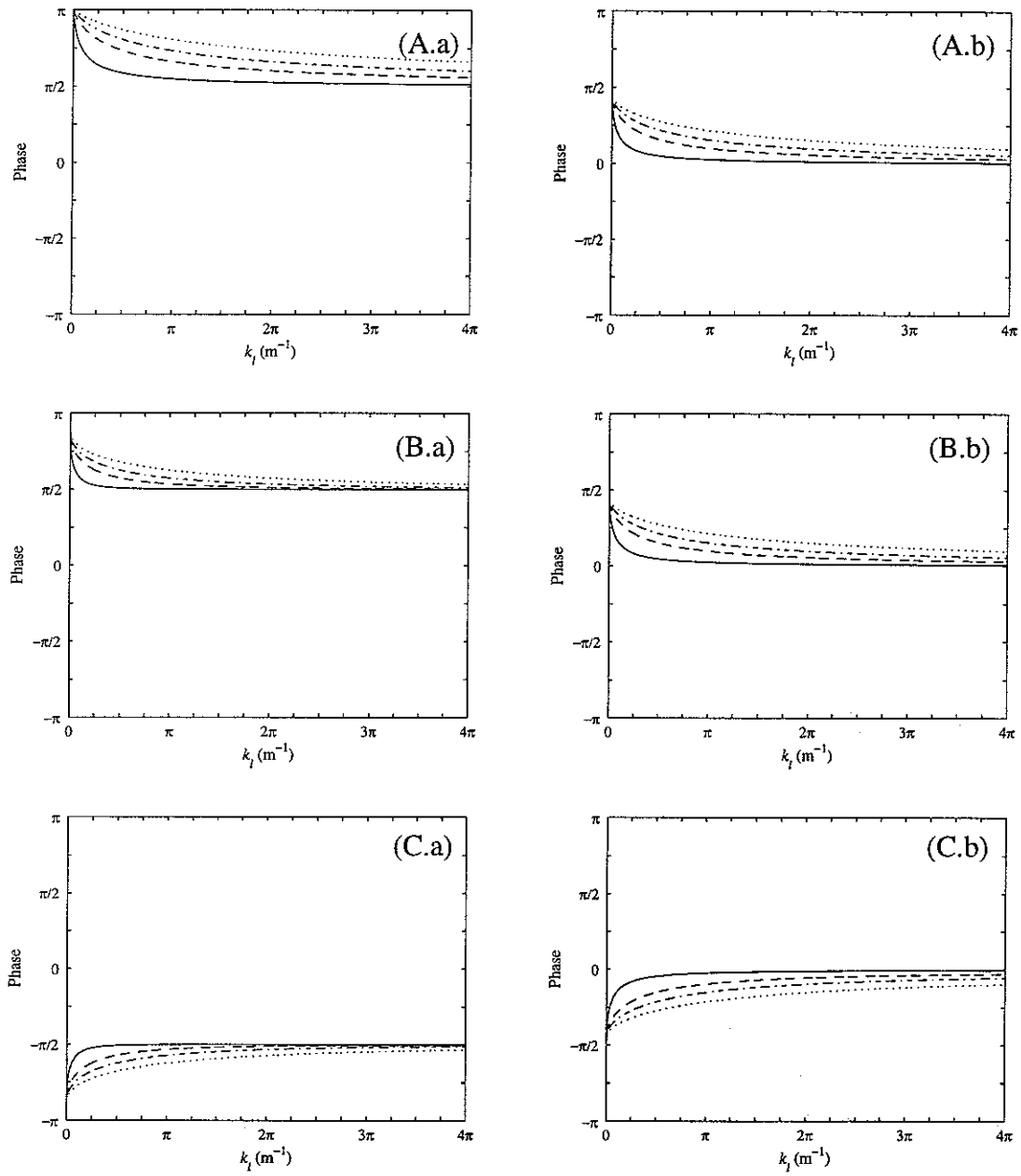

Figure 15. Phases of reflection and transmission coefficients for the junction of a uniform bar and a non-uniform bar with cross-sectional area satisfying equation (2.11) and $\mu = 1$: the connection is (A) the type-A, (B) the type-B, and (C) the type-C in Figure 12; (a) phase of reflection coefficient, (b) phase of transmission coefficient;

——— , $\alpha = 1$; ------ , $\alpha = 5$; ·-·-·- , $\alpha = 10$; ····· , $\alpha = 20$.

2.7 Summary

In this section wave methods have been developed for axial motion of a non-uniform bar with polynomial variation in cross-sectional area. Analytical expressions for the displacement, internal force and propagation matrices for the non-uniform bar have been derived. By using matrices, wave generation by an external force, reflection at a boundary and reflection/transmission at a discontinuity have been investigated. The results can be used to predict the responses of more complex, built-up structures as will be illustrated in section 4.

Throughout the work, it was seen that the non-uniformity can be considered as additional stiffness. For example, when an end of a non-uniform bar is excited by an external force, non-uniformity of the bar makes the amplitude of the induced wave smaller than that in a uniform bar and the phase lag is not $\frac{\pi}{2}$. The influence of the non-uniformity is greatest at low frequencies and becomes smaller as frequency increases.

It should also be noticed that non-uniform bars are not symmetric. For example, when an end of a non-uniform bar is excited by an external force, the phases of the induced waves at the left- and right-hand end are different.

In section 2.6, reflection and transmission at a junction between a uniform bar and a non-uniform bar with linearly variable thickness were investigated on the three connection types in detail. It was shown that the phases of the reflection coefficients of the type-B and type-C connections are opposite, which implies that there will be no change in the phase of a wave undergoing the two reflections.

3. BENDING WAVES IN A NON-UNIFORM BEAM

3.1 Introduction

In the previous section, wave methods were developed for axial motion of a non-uniform bar. A similar approach is applied to bending motion of a non-uniform beam in this section. However, care should be taken because nearfield waves exist in bending motion and bending waves are dispersive.

It is shown that bending motion of a non-uniform Euler-Bernoulli beam with polynomial variations in cross-sectional area and the second moment of area such that $A(x) \propto x^{\mu}$ and $I(x) \propto x^{\mu+2}$, with μ real and non-negative, can be analysed by the wave method. In particular, this case includes a rectangular beam with linearly variable thickness and constant width.

In section 3.2, bending motion of a non-uniform beam is reviewed. It is shown that, if the beam has polynomial variations in cross-sectional area and the second moment of area such that $A(x) \propto x^{\mu}$ and $I(x) \propto x^{\mu+2}$, the motion can be expressed as a linear combination of Hankel functions and modified Bessel functions.

In section 3.3, the results of section 3.2 are reformulated in terms of waves. Propagation, displacement and internal force matrices are derived for a non-uniform beam and asymptotic behaviour of the matrices is investigated.

In section 3.4, bending wave generation in non-uniform beams by external forces and moments is investigated and, in section 3.5, reflection at an end of the non-uniform beams is investigated.

In section 3.6, reflection and transmission matrices at a discontinuity are defined. In particular, reflection and transmission at a junction between a uniform beam and a non-uniform beam are investigated in detail.

The results are subsequently used in the numerical examples in section 4.

3.2 Governing equation and its solution

The flexural displacement $w(x,t)$ for the free vibration of an Euler-Bernoulli beam is governed by the differential equation

$$\frac{\partial^2}{\partial x^2}\left[EI\frac{\partial^2 w}{\partial x^2}\right]+\rho A\frac{\partial^2 w}{\partial t^2}=0 \tag{3.1}$$

where EI is the bending stiffness or flexural rigidity and ρA is the mass per unit length with E being the modulus of elasticity, I the second moment of area, ρ the density and A the cross-sectional area.

Consider a beam of which the material properties, ρ and E, are constant but the geometric properties, A and I, are variable such that

$$\begin{aligned} A(x) &= A_0\left(1+\frac{x}{x_0}\right)^{\mu} \\ I(x) &= I_0\left(1+\frac{x}{x_0}\right)^{\mu+2} \end{aligned} \tag{3.2a,b}$$

where A_0 and I_0 are the cross-sectional area and the second moment of area at $x=0$, respectively. In equations (3.2), it should be noticed that x_0 is the same constant for both $A(x)$ and $I(x)$.

When the time dependence of the displacement $w(x,t)$ is of the form $e^{i\omega t}$, suppressed here for clarity, equation (3.1) for the beam can be expanded as

$$\xi^2\frac{d^4w}{d\xi^4}+2(\mu+2)\xi\frac{d^3w}{d\xi^3}+(\mu+1)(\mu+2)\frac{d^2w}{d\xi^2}-k_{b,0}^4x_0^2w=0 \tag{3.3}$$

where $\xi=x+x_0$ and

$$k_{b,0}=\sqrt[4]{\frac{\rho A_0\omega^2}{EI_0}} \tag{3.4}$$

is the wavenumber of bending waves at $x=0$.

Equation (3.3) is identical to equation (B.16) if $\mu=\nu$ and $k=k_{b,0}\sqrt{x_0}$. Accordingly, the displacement of the beam can be written as

$$w(x)=\left(\frac{1}{\xi}\right)^{\nu/2}\left\{C_1H_\nu^{(2)}(\phi)+C_2K_\nu(\phi)+C_3H_\nu^{(1)}(\phi)+C_4I_\nu(\phi)\right\} \tag{3.5}$$

where $\phi=2k_{b,0}\sqrt{\xi x_0}$. The slope $\frac{\partial w}{\partial x}$, shear force Q and bending moment M, defined as shown in Figure 16, are thus given by

$$\frac{\partial w}{\partial x}=\left(\frac{1}{\xi}\right)^{\frac{\nu+1}{2}}\left\{-C_1H_\nu^{(2)}(\phi)-C_2K_\nu(\phi)\ -C_3H_\nu^{(1)}(\phi)+C_4I_\nu(\phi)\right\} \tag{3.6}$$

$$\begin{aligned} Q&=\frac{d}{dx}\left(EI(x)\frac{d^2w}{dx^2}\right)\\ &=EI_0\left(\frac{1}{\xi}\right)^{\frac{\nu+3}{2}}\left\{C_1H_{\nu+1}^{(2)}(\phi)-C_2K_{\nu+1}(\phi)+C_3H_{\nu+1}^{(1)}(\phi)+C_4I_{\nu+1}(\phi)\right\} \end{aligned} \tag{3.7a, b}$$

$$\begin{aligned} M&=-EI(x)\frac{d^2w}{dx^2}\\ &=-EI_0\left(\frac{1}{\xi}\right)^{\frac{\nu+2}{2}}\left\{C_1H_{\nu+2}^{(2)}(\phi)a^{+}+C_2K_{\nu+2}(\phi)+C_3H_{\nu+2}^{(1)}(\phi)+C_4I_{\nu+2}(\phi)\right\} \end{aligned} \tag{3.8a, b}$$

where C_1, C_2, C_3 and C_4 are arbitrary constants.

Many different beams exist whose geometries satisfy equation (3.2). One of these is a rectangular beam which has thickness h and width b such that

$$h(x)=h_0(1+\alpha x), \qquad b(x)=b_0(1+\alpha x)^{\mu-1} \tag{3.9a,b}$$

where b_0, h_0 and α are constants which satisfy $A_0=b_0h_0$, $I_0=\frac{b_0h_0^3}{12}$ and $x_0=\frac{1}{\alpha}$.

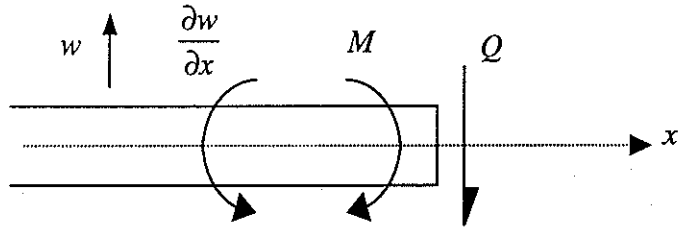

Figure 16. Notation of positive slope, shear force and bending moment.

3.3 The wave description

Equations (3.5) to (3.8) can be described using the wave formulation which has been introduced in appendix A.1. The displacement and internal force vectors at a section of the beam can then be written as

$$\mathbf{w}=\begin{Bmatrix} w \\ \partial w/\partial x \end{Bmatrix}=\Psi^{+}\mathbf{a}^{+}+\Psi^{-}\mathbf{a}^{-} \tag{3.10}$$

$$\mathbf{f} = \begin{Bmatrix} Q \\ M \end{Bmatrix} = \Phi^{+}\mathbf{a}^{+} + \Phi^{-}\mathbf{a}^{-} \tag{3.11}$$

where

$$\mathbf{a}^{+} = \begin{Bmatrix} a^{+} \\ a_N^{+} \end{Bmatrix}, \qquad \mathbf{a}^{-} = \begin{Bmatrix} a^{-} \\ a_N^{-} \end{Bmatrix} \tag{3.12a,b}$$

$$\Psi^{+} = \begin{bmatrix} 1 & 1 \\ -(k_{b,0})\dfrac{H_{\nu+1}^{(2)}(2k_{b,0}x_0)}{H_{\nu}^{(2)}(2k_{b,0}x_0)} & -(k_{b,0})\dfrac{K_{\nu+1}(2k_{b,0}x_0)}{K_{\nu}(2k_{b,0}x_0)} \end{bmatrix}$$

$$\Psi^{-} = \begin{bmatrix} 1 & 1 \\ -(k_{b,0})\dfrac{H_{\nu+1}^{(1)}(2k_{b,0}x_0)}{H_{\nu}^{(1)}(2k_{b,0}x_0)} & (k_{b,0})\dfrac{I_{\nu+1}(2k_{b,0}x_0)}{I_{\nu}(2k_{b,0}x_0)} \end{bmatrix} \tag{3.13a,b}$$

$$\Phi^{+} = EI_0 \begin{bmatrix} (k_{b,0})^3 \dfrac{H_{\nu+1}^{(2)}(2k_{b,0}x_0)}{H_{\nu}^{(2)}(2k_{b,0}x_0)} & -(k_{b,0})^3 \dfrac{K_{\nu+1}(2k_{b,0}x_0)}{K_{\nu}(2k_{b,0}x_0)} \\ -(k_{b,0})^2 \dfrac{H_{\nu+2}^{(2)}(2k_{b,0}x_0)}{H_{\nu}^{(2)}(2k_{b,0}x_0)} & -(k_{b,0})^2 \dfrac{K_{\nu+2}(2k_{b,0}x_0)}{K_{\nu}(2k_{b,0}x_0)} \end{bmatrix}$$

$$\Phi^{-} = EI_0 \begin{bmatrix} (k_{b,0})^3 \dfrac{H_{\nu+1}^{(1)}(2k_{b,0}x_0)}{H_{\nu}^{(1)}(2k_{b,0}x_0)} & (k_{b,0})^3 \dfrac{I_{\nu+1}(2k_{b,0}x_0)}{I_{\nu}(2k_{b,0}x_0)} \\ -(k_{b,0})^2 \dfrac{H_{\nu+2}^{(1)}(2k_{b,0}x_0)}{H_{\nu}^{(1)}(2k_{b,0}x_0)} & -(k_{b,0})^2 \dfrac{I_{\nu+2}(2k_{b,0}x_0)}{I_{\nu}(2k_{b,0}x_0)} \end{bmatrix} \tag{3.14a,b}$$

and the propagation matrices are defined by

$$\mathbf{F}^{+}(x) = \left(\frac{x_0}{x+x_0}\right)^{\frac{\nu}{2}} \begin{bmatrix} \dfrac{H_{\nu}^{(2)}\left(2k_{b,0}\sqrt{x_0(x+x_0)}\right)}{H_{\nu}^{(2)}(2k_{b,0}x_0)} & 0 \\ 0 & \dfrac{K_{\nu}\left(2k_{b,0}\sqrt{x_0(x+x_0)}\right)}{K_{\nu}(2k_{b,0}x_0)} \end{bmatrix}$$

$$\mathbf{F}^{-}(x) = \left(\frac{x_0}{x+x_0}\right)^{\frac{\nu}{2}} \begin{bmatrix} \dfrac{H_{\nu}^{(1)}\left(2k_{b,0}\sqrt{x_0(x+x_0)}\right)}{H_{\nu}^{(1)}(2k_{b,0}x_0)} & 0 \\ 0 & \dfrac{I_{\nu}\left(2k_{b,0}\sqrt{x_0(x+x_0)}\right)}{I_{\nu}(2k_{b,0}x_0)} \end{bmatrix} \tag{3.15a,b}$$

Using equations (B.57), (B.58), (B.62) and (B.65), the displacement and internal force matrices asymptote to those of a uniform beam with the area A_0 and the second moment of area I_0 when $k_{b,0}x_0 \gg 1$. Also, the phase θ of F_{11}^{+} (element (1,1) of $\mathbf{F}^{+}$) asymptotes to

$$\theta \approx -\left(2k_{b,0}\sqrt{x_0(x+x_0)} - 2k_{b,0}x_0\right) \tag{3.16}$$

when $k_{b,0}x_0 \gg 1$. If a wave propagates over a length L then, since the wavenumber $k_{b,L}$ at $x = L$ is given by

$$k_{b,L} = \frac{k_{b,0}}{\sqrt{1+\dfrac{L}{x_0}}} \tag{3.17}$$

the phase change is given by

$$\theta \propto -k_{b,m}L \tag{3.18}$$

where the wavenumber $k_{b,m}$ is defined by

$$k_{b,m} = \frac{2k_{b,0}k_{b,L}}{k_{b,0}+k_{b,L}} \tag{3.19}$$

In terms of the wavelength λ, equation (3.19) can be expressed as

$$\lambda_{b,m} = \frac{\lambda_{b,0}+\lambda_{b,L}}{2} \tag{3.20}$$

Thus the effective mean wavelength is the mean of the wavelengths at the ends of the propagation length. In the same way, when $k_{b,0}x_0 \gg 1$,

$$\begin{aligned}
\mathbf{F}_{0\to L}^{+} &\approx \left(\frac{x_0}{L+x_0}\right)^{\frac{\nu}{2}+\frac{1}{4}} \begin{bmatrix} e^{-ik_{b,m}L} & 0 \\ 0 & e^{-k_{b,m}L} \end{bmatrix} \\
\mathbf{F}_{L\to 0}^{-} &\approx \left(\frac{L+x_0}{x_0}\right)^{\frac{\nu}{2}+\frac{1}{4}} \begin{bmatrix} e^{-ik_{b,m}L} & 0 \\ 0 & e^{-k_{b,m}L} \end{bmatrix}
\end{aligned} \tag{3.21a, b}$$

Thus wave propagation in a non-uniform beam can be simplified as shown by equation (3.21) using the mean wavenumber $k_{b,m}$ in the high frequency region. Furthermore, the propagation matrices asymptote to those of the uniform waveguide with the wavenumber $k_{b,0}$ when the non-uniformity of the waveguide is very small, i.e., $x_0 \gg L$.

3.4 Wave generation by local excitation

Consider a non-uniform beam with geometry satisfying equation (3.2), an end of which is excited by a harmonic force vector $\mathbf{f}_{ext}e^{i\omega t}$. When the left-hand end of the beam is excited as shown in Figure 17, $\mathbf{q}^+$ can be obtained by combining equations (3.13) and (3.14) with equation (A.11) and, when the right-hand end of the beam is excited as shown in Figure 18, $\mathbf{q}^-$ can be obtained by combining equations (3.13) and (3.14) with equation (A.12). Since the expressions are too complicated to show them explicitly, the results are shown graphically.

When a section of the beam is excited as shown in Figure 19, $\mathbf{q}^+$ and $\mathbf{q}^-$ can be obtained by combining equations (3.13) and (3.14) with equation (A.15) and by combining equations (3.13) and (3.14) with equation (A.16), respectively.

Figure 20 shows waves generated in a non-uniform beam with the geometry satisfying equation (3.9) and $\mu = 1$, an end of which is excited by a local force. First of all, it can be seen that the induced waves asymptote to that in a uniform beam at high frequencies. However, unlike in the case of axial waves, the amplitudes of the induced waves at the left-hand end are not identical to those at the right-hand end. Moreover, the amplitudes at the left-hand end are greater than those at the right-hand end. Meanwhile, it should be noted that the amplitude of the nearfield component at the right-hand end is quite high and tends to infinity as $k_{b,0} \to 0$. Figure 21 shows waves generated by a local moment. It can be seen that the amplitudes at the right-hand end are greater than those at the left-hand end. It is due to the fact that the bending stiffness of the left-hand side is less than that of the right-hand side.

Figure 22 shows waves generated in a non-uniform beam with geometry satisfying equation (3.9) and $\mu = 1$, a section of which is excited by a local force as in Figure 19. In the figure, the phases of the nearfield components are equal to $-\pi$. First of all, it can be seen that the positive- and negative-going waves are identical. However, unlike the uniform beam where energy is equally distributed in each component, the amplitude of the propagating component is not same as that of the nearfield component. It can also be noted that the amplitudes of the propagating components in both cases tend to infinity as $k_{b,0} \to 0$. Figure 23 shows waves generated by a local moment. In the figure, the phase of the nearfield component of the positive-going waves is equal to π. It can be seen that the amplitudes of

the propagating components are identical but the phases of the positive-going waves are π minus the phases of the negative-going waves.

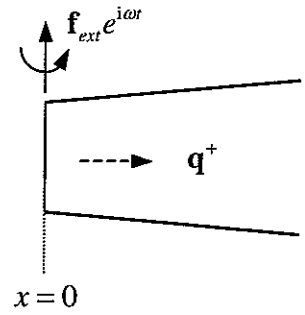

Figure 17. Non-uniform beam, left-hand end of which is excited by local forces.

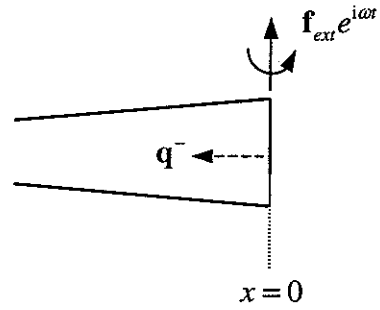

Figure 18. Non-uniform beam, right-hand end of which is excited by local forces.

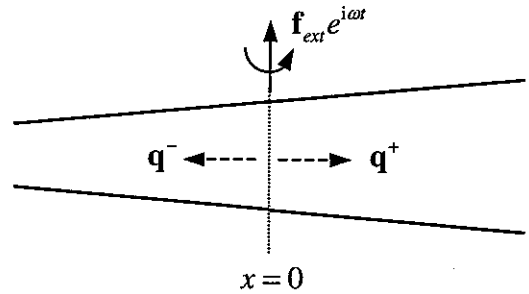

Figure 19. Non-uniform beam, a section of which is excited by local forces.

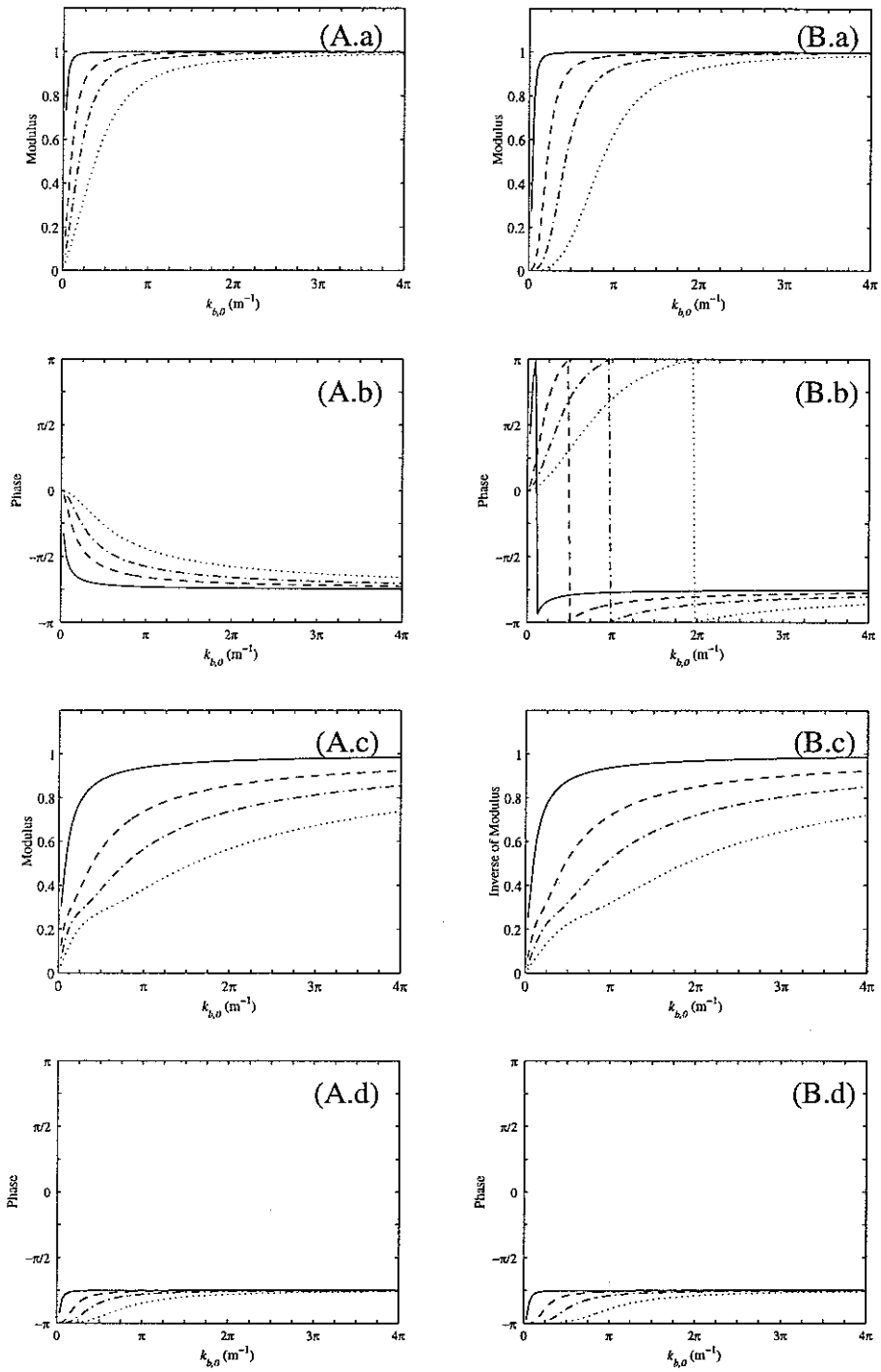

Figure 20. Bending wave generation in a non-uniform beam with geometry satisfying equation (3.9) and $\mu = 1$, when (A) the left- and (B) the right-hand end is excited by a force: (a) ratio of the amplitude of the propagating component of the induced waves to that in the uniform beam, (b) phase of the propagating component, (c) ratio or inverse of ratio of the amplitude of the nearfield component to that in the uniform beam, and (d) phase of the nearfield component;

——— , $\alpha = 0.1$; - - - - - - , $\alpha = 0.5$; - · - · - · , $\alpha = 1$; ····· , $\alpha = 2$.

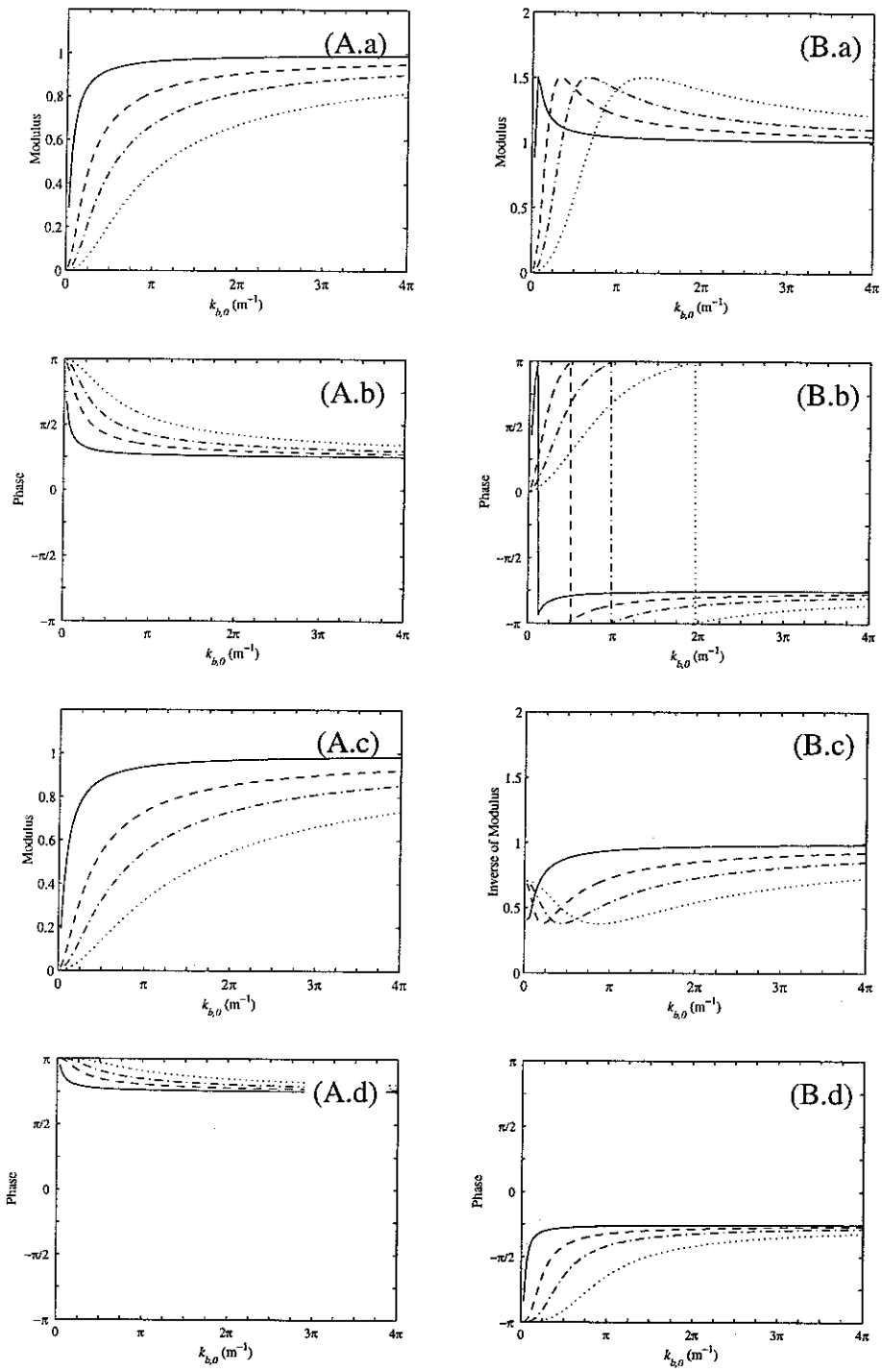

Figure 21. Bending wave generation in a non-uniform beam with geometry satisfying equation (3.9) and $\mu = 1$, when (A) the left- and (B) the right-hand end is excited by a moment: (a) ratio of the amplitude of the propagating component of the induced waves to that in the uniform beam, (b) phase of the propagating component, (c) ratio or inverse of ratio of the amplitude of the nearfield component to that in the uniform beam and (d) phase of the nearfield component;

——— , $\alpha = 0.1$; ------ , $\alpha = 0.5$; - - - - - , $\alpha = 1$; ..... , $\alpha = 2$.

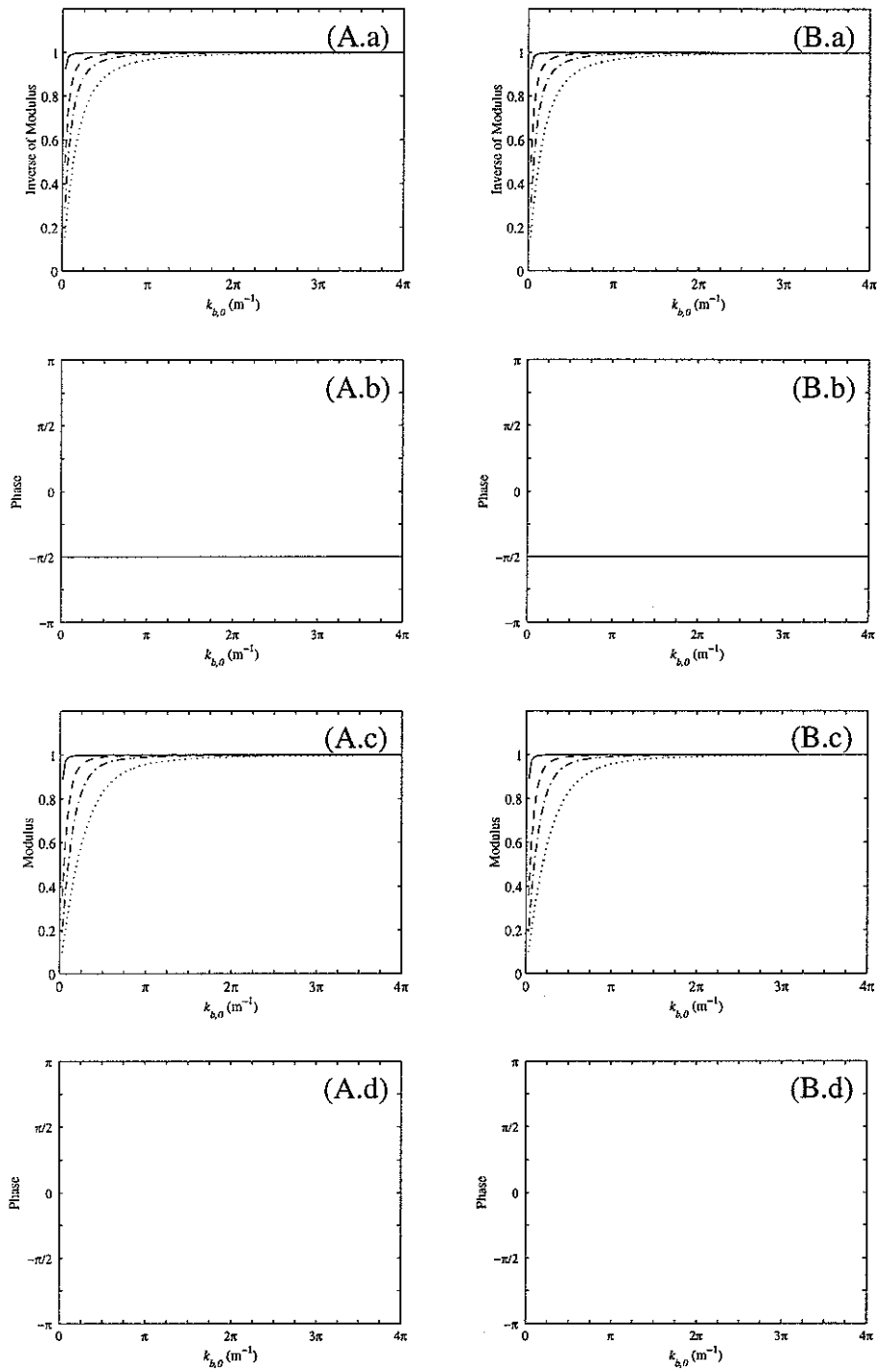

Figure 22. Bending wave generation in a non-uniform beam with geometry satisfying equation (3.9) and $\mu = 1$, a section of which is excited by a force: (A) positive-going waves and (B) negative-going waves; (a) inverse of ratio of the amplitude of the propagating component to that in the uniform beam, (b) phase of the propagating component, (c) ratio of the amplitude of the nearfield component to that in the uniform beam, (d) phase of the nearfield component;

——— , $\alpha = 0.1$; ------ , $\alpha = 0.5$; - - - - - , $\alpha = 1$; ····· , $\alpha = 2$.

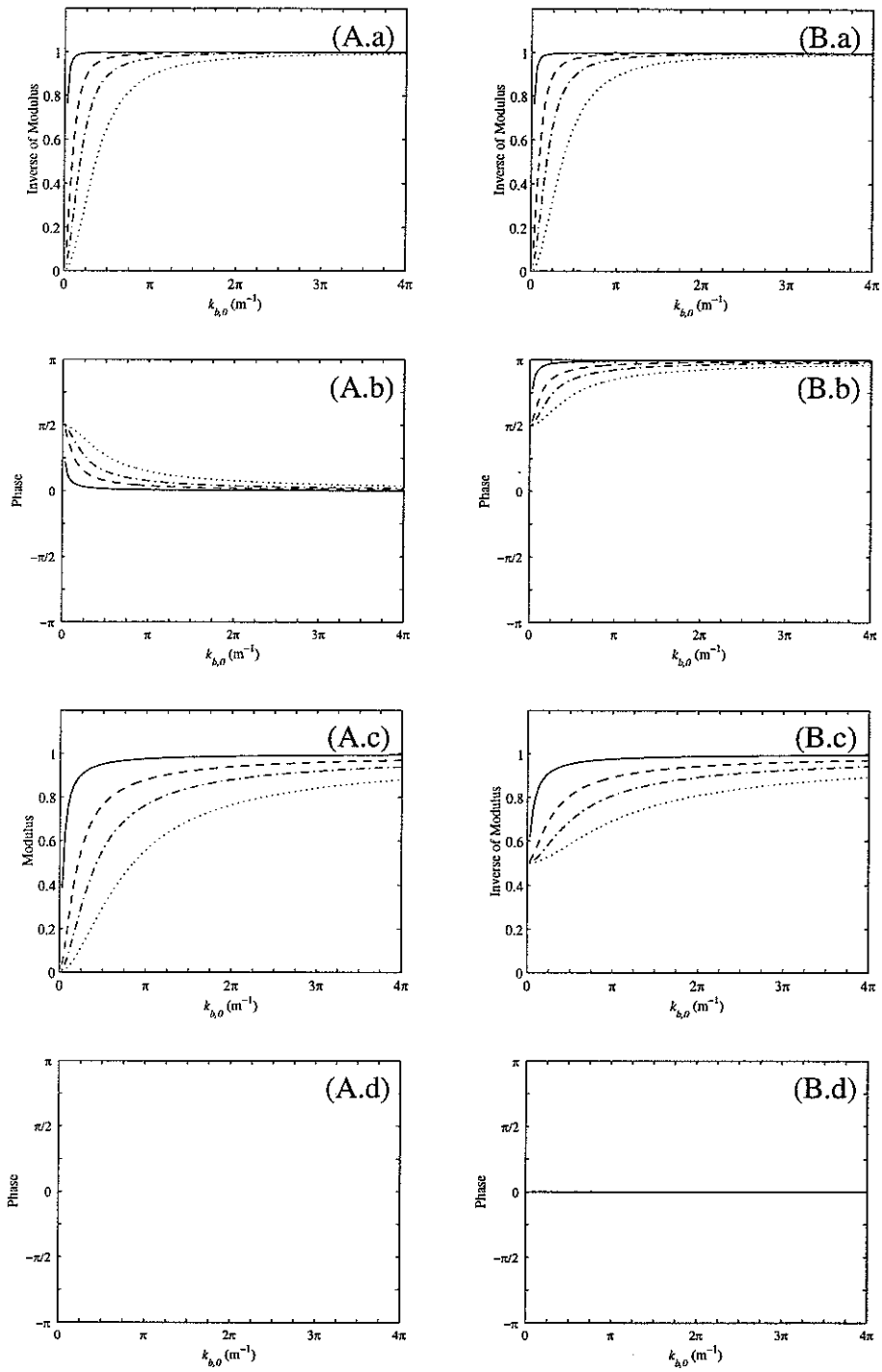

Figure 23. Bending wave generation in a non-uniform beam with geometry satisfying equation (3.9) and $\mu = 1$, a section of which is excited by a moment: (A) positive-going waves and (B) negative-going waves; (a) inverse of ratio of the amplitude of the propagating component to that in the uniform beam, (b) phase of the propagating component, (c) ratio or inverse of ratio of the amplitude of the nearfield component to that in the uniform beam, (d) phase of the nearfield component;

——— , $\alpha = 0.1$; ------ , $\alpha = 0.5$; ------- , $\alpha = 1$; ..... , $\alpha = 2$.

3.5 Reflection at a boundary

The reflection matrix **R** at an end of a waveguide is in general given by equation (A.20). If equations (A.20), (3.13) and (3.14) are combined, the reflection matrix **R** at an end of a non-uniform beam with geometry satisfying equation (3.2) as shown in Figure 24 can be obtained. Since the expressions are too complicated to state them explicitly, here the results are shown graphically.

Figure 25 shows the phases of R_{11} (the (1,1) element of **R**) at free, clamped and simply supported ends of a non-uniform beam with geometry satisfying equation (3.9) and $\mu = 1$. It can be seen that the phases asymptote to those of the uniform beam while, unlike the axial wave, symmetry between the left- and right-hand cases does not hold. It can also be seen that the influence of the non-uniformity at the clamped end is smaller than those at other boundaries.

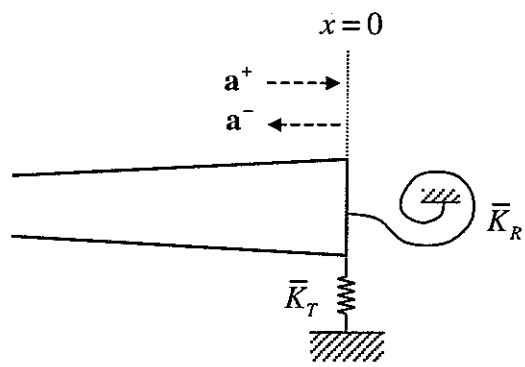

Figure 24. Non-uniform beam with right-hand boundary supported by external dynamic stiffnesses.

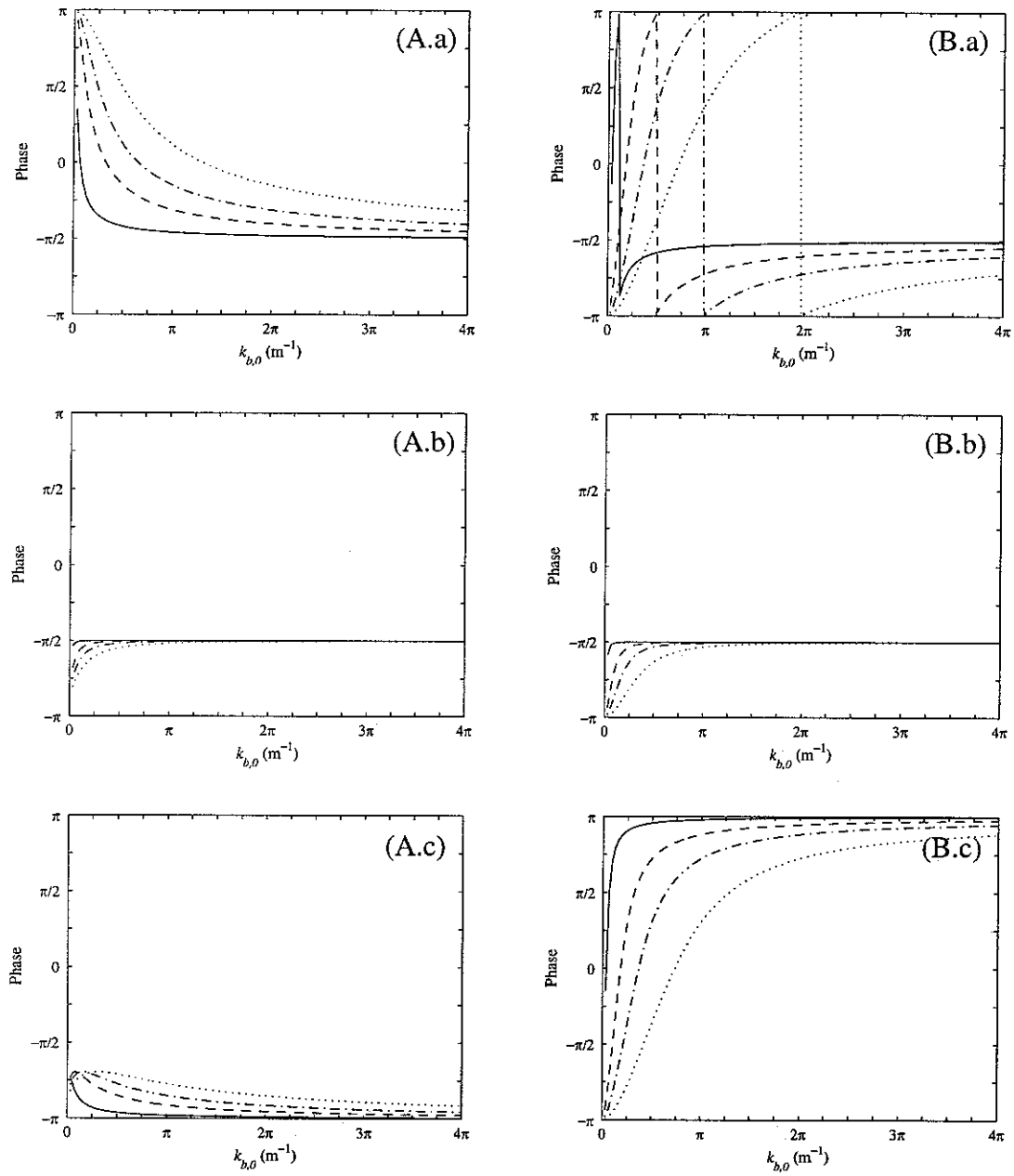

Figure 25. Phase of R_{11} for a boundary of a non-uniform beam with geometry satisfying equation (3.9) and $\mu = 1$ at the (A) left- and (B) right-hand end: (a) free, (b) clamped and (c) simply supported boundary condition;

——— , $\alpha = 0.1$; ------ , $\alpha = 0.5$; -·-·-·- , $\alpha = 1$; ····· , $\alpha = 2$.

3.6 Reflection and transmission at a discontinuity

The reflection and the transmission matrices **R** and **T** at a discontinuity in a section of a waveguide are given in the general case by equations (A.29) and (A.30), respectively. If equations (A.29), (A.30), (3.13) and (3.14) are combined, **R** and **T** at a junction of two non-uniform beams with geometry satisfying equation (3.2) as shown in Figure 26 can be obtained. Since the expressions are too complicated to state explicitly, here the results are shown graphically.

As shown in Figure 12, three connection types between a uniform beam and a non-uniform beam can be considered when $A_{0,a} = A_{0,b}$ and $I_{0,a} = I_{0,b}$. Figures 27, 28 and 29 show reflection and transmission coefficient for the three connections when the non-uniform beam has geometry satisfying equation (3.9) and $\mu = 1$. It can be seen that the power coefficients of the type-A and type-B junctions are identical and the phases of T_{11} are also identical. It should be recalled that the type-A and type-B junctions are symmetric about $x = 0$. Meanwhile, it should also be noted that the phase of R_{11} of the type-B is the opposite of that of the type-C.

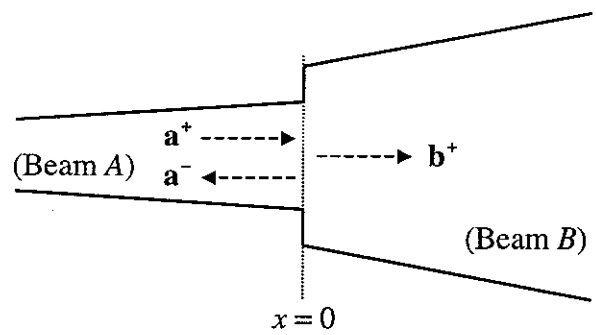

Figure 26. Connection of two non-uniform beams with different geometry.

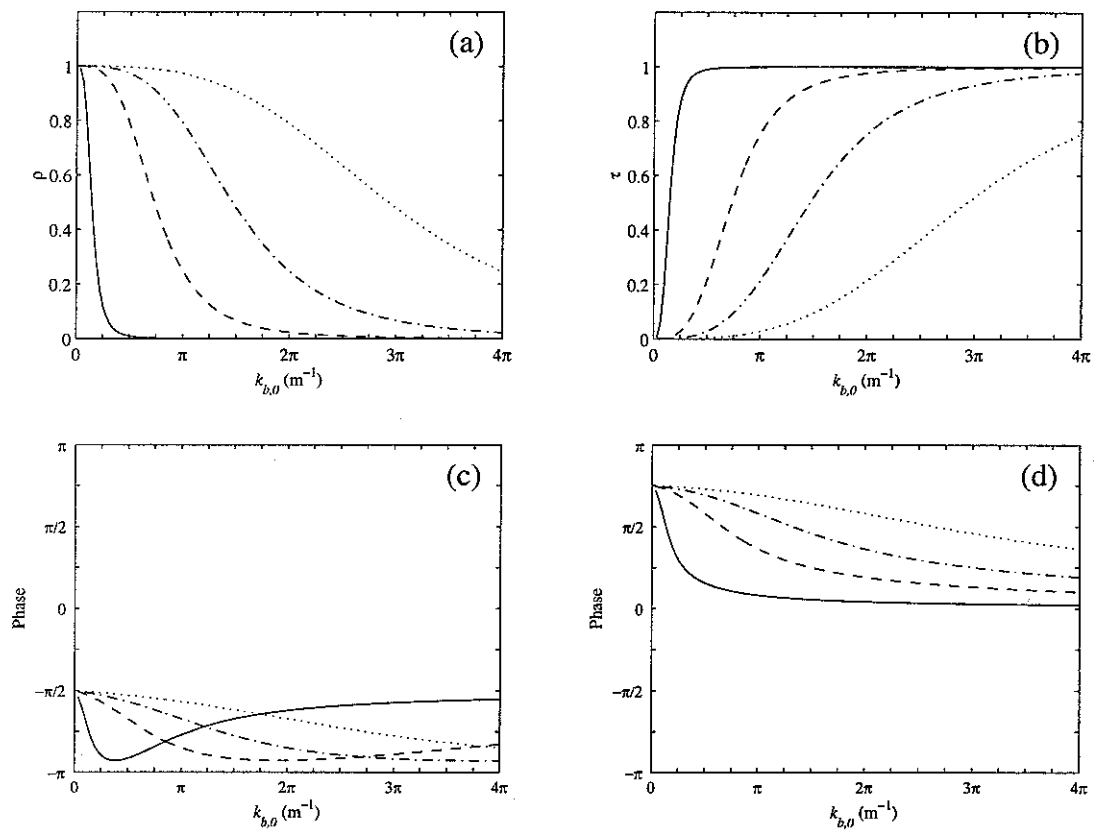

Figure 27. Reflection and transmission at the connection type-A of a uniform beam and a non-uniform beam with geometry satisfying equation (3.9) and $\mu = 1$: (a) power reflection coefficient, (b) power transmission coefficient, (c) phase of R_{11}, and (d) phase of T_{11};

——— , $\alpha = 1$; ------ , $\alpha = 5$; -·-·-· , $\alpha = 10$; ····· , $\alpha = 20$.

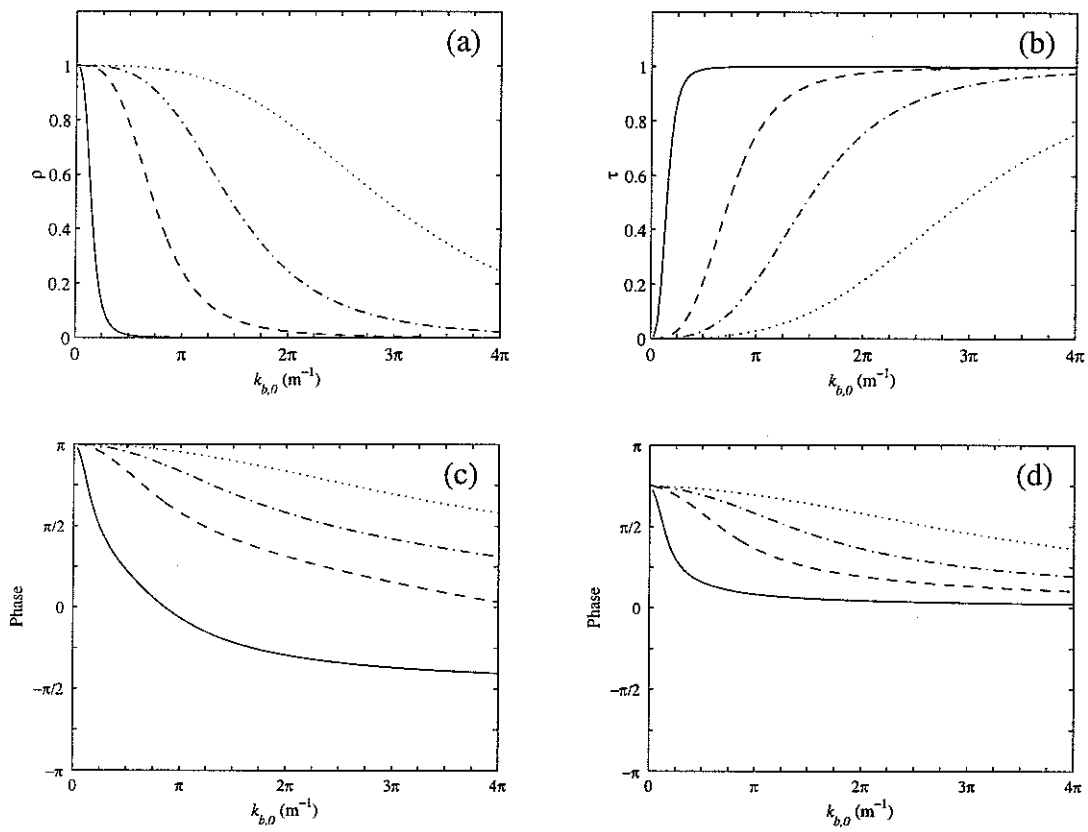

Figure 28. Reflection and transmission at connection type-B of a uniform beam and a non-uniform beam with geometry satisfying equation (3.9) and $\mu = 1$: (a) Power reflection coefficient, (b) power transmission coefficient, (c) phase of R_{11}, and (d) phase of T_{11}: ——— , $\alpha = 1$; ------ , $\alpha = 5$; -·-·-·- , $\alpha = 10$; ····· , $\alpha = 20$.

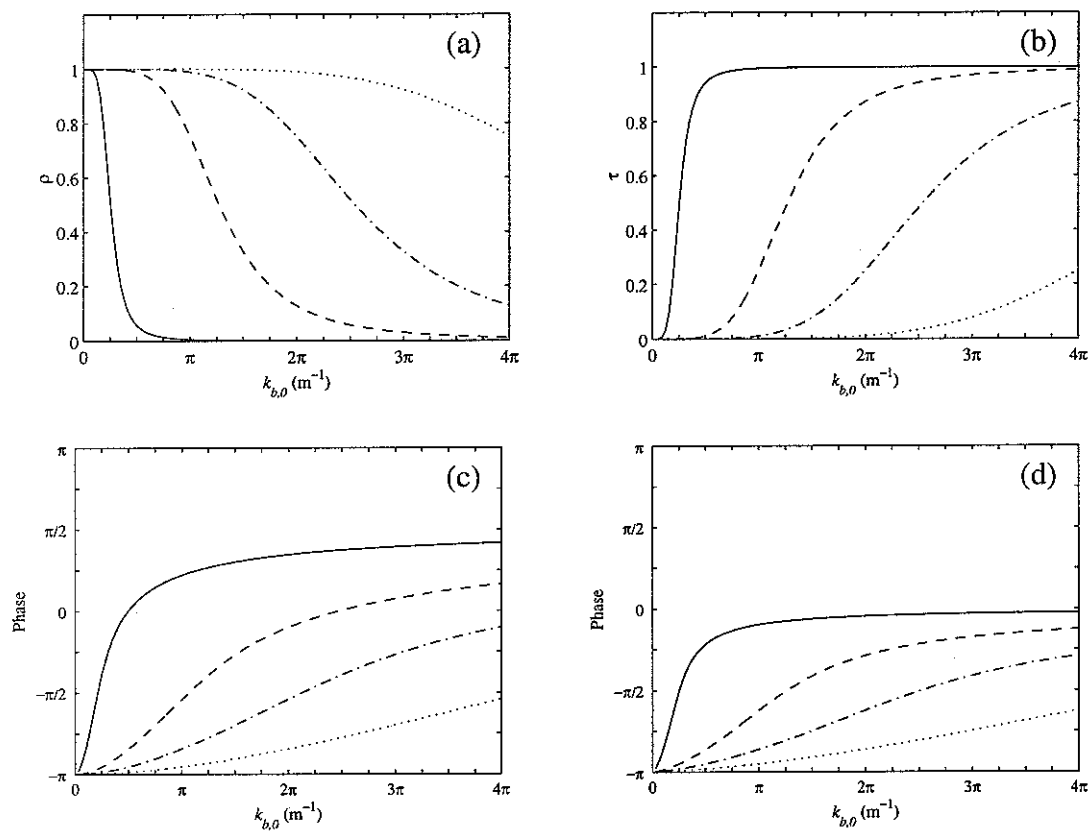

Figure 29. Reflection and transmission at the connection type-C of a uniform beam and a non-uniform beam with geometry satisfying equation (3.9) and $\mu = 1$: (a) Power reflection coefficient, (b) power transmission coefficient, (c) phase of R_{11}, and (d) phase of T_{11}:

——— , $\alpha = 1$; ------ , $\alpha = 5$; -·-·-·- , $\alpha = 10$; ····· , $\alpha = 20$.

3.7 Summary

In this section wave methods have been applied to bending motion of a non-uniform Euler-Bernoulli beam with a polynomial variation in cross-sectional area and the second moment of area such that $A(x) \propto x^{\mu}$ and $I(x) \propto x^{\mu+2}$. Analytical expressions for the displacement, internal force and propagation matrices for a non-uniform beam were derived. By using the matrices, wave generation by an external force, reflection at a boundary and reflection/transmission at a discontinuity were investigated. The results can be used to predict the responses of more complex, built-up structures as illustrated in section 4.

The results were much more complicated due to the existence of the nearfield waves. However, the trend that the behaviour of the non-uniform beam asymptotes to that of the uniform beam as frequency increases was observed in each case investigated. Care should also be taken since bending waves are dispersive. For example, it was shown that phase change in propagation path with length L asymptotes to $k_{b,m}L$ in high frequency region where $k_{b,m}$ represents the effective wavenumber of the propagation path.

In section 3.6, the reflection and transmission at a junction between a uniform beam and a non-uniform beam were investigated in detail. It was shown that the phases of R_{11} of the type-B and the type-C are opposite, which implies that there will be no change in the phase of the propagating component when a wave undergoes the two reflections.

4. APPLICATIONS

4.1 Introduction

The wave methods for a non-uniform waveguide, developed in sections 2 and 3, can be usefully applied to many cases. One of the most important cases concerns transmission through a connector which connects two uniform waveguides. In general, a connector might be used to improve transmission efficiency by preventing rapid impedance change. In section 4.2, the reflection and transmission matrices of a connector are developed and the effect of the connector on wave propagation is investigated.

In the second example, a comparison is made between an exact result using the approach developed in this report and approximate results obtained by discrete wave models. The discrete wave model is used to analyse motion of a continuous non-uniform waveguide assuming that the non-uniform waveguide is composed of short, uniform sections. Since this approach is not exact, errors due to discretization always exists even though the error can be reduced by increasing the number of uniform sections. Moreover, increasing the number of the uniform sections causes another difficulty in that more computational power and time are required. These problems can be avoided by using the wave methods developed here.

4.2 Reflection and transmission through a connector

Consider a linearly tapered waveguide with length L which connects two different semi-infinite uniform waveguides as shown in Figure 30. For simplicity, the waveguides and connector are all assumed to have same material properties and a rectangular cross-section. The connector is tapered only in its thickness and, thus, the cross-sectional area A and second moment of area I of the connector are given by

$$A(x) = A_0\left(1+\frac{\alpha}{L}x\right)$$
$$I(x) = I_0\left(1+\frac{\alpha}{L}x\right)^3 \qquad (4.1a,b)$$

where α is the taper rate, A_0 is cross-sectional area and I_0 is the second moment of area at $x=0$. Equation (4.1) satisfies the conditions given by equations (2.5) and (3.2) if $\mu=1$ and

$$x_0 = \frac{L}{\alpha} \tag{4.2}$$

Therefore transmission of axial and bending waves through the connector can be analysed by the wave methods developed in sections 2 and 3.

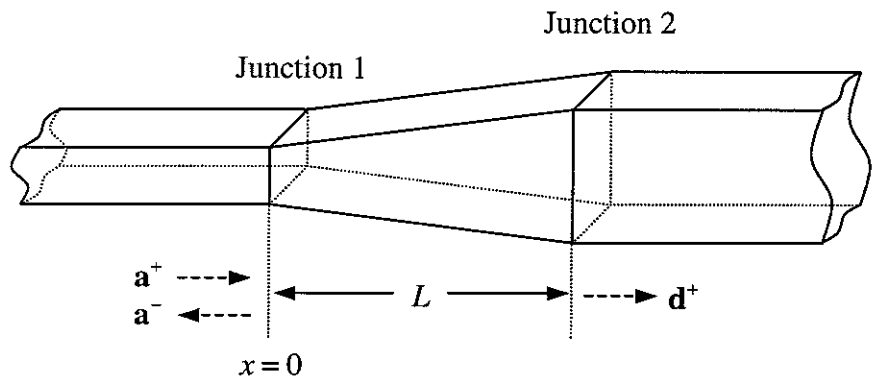

Figure 30. A rectangular connector tapered in thickness.

When a wave vector $\mathbf{a}^+$ is incident from the left-hand side of the junction 1, the amplitudes of the reflected and transmitted waves, $\mathbf{a}^-$ and $\mathbf{d}^+$, can be given in terms of the reflection and transmission matrices, $\mathbf{R}_T$ and $\mathbf{T}_T$, for the connector such that

$$\mathbf{a}^- = \mathbf{R}_T\mathbf{a}^+, \qquad \mathbf{d}^+ = \mathbf{T}_T\mathbf{a}^+ \tag{4.3a, b}$$

$\mathbf{R}_T$ and $\mathbf{T}_T$ are given in terms of the reflection and transmission matrices at the two junctions such that [24]

$$\begin{aligned} \mathbf{R}_T &= \mathbf{R}_1 + \hat{\mathbf{T}}_1\mathbf{F}^-\mathbf{R}_2\mathbf{F}^+[\mathbf{I} - \hat{\mathbf{R}}_1\mathbf{F}^-\mathbf{R}_2\mathbf{F}^+]^{-1}\mathbf{T}_1, \\ \mathbf{T}_T &= \mathbf{T}_2\mathbf{F}^+[\mathbf{I} - \hat{\mathbf{R}}_1\mathbf{F}^-\mathbf{R}_2\mathbf{F}^+]^{-1}\mathbf{T}_1, \end{aligned} \tag{4.4a, b}$$

where the subscripts 1 and 2 refer to the junctions, respectively, and the superscript $\cap$ refers to the case where waves are incident from the right-hand side of the junction. If equation (4.4) is combined with the reflection and transmission matrices developed in section 2.6 and 3.6, $\mathbf{R}_T$ and $\mathbf{T}_T$ for the connector can be obtained.

Figure 31 shows the reflection and transmission coefficients for an axial wave incident on the connector. It can be seen that, as the taper rate α increases, the power transmission coefficient decreases. However, when $k_l L \gg 0$, the power transmission coefficient tends to 1 and phase of the transmission coefficient, θ_t, asymptotes to $-k_l L$.

These results can be understood by considering two extreme cases. The first is the case where there is no geometric variation among two uniform waveguides and the connector. This is just a uniform case where $\tau = 1$ and $\theta_t = -k_l L$. These phenomena can be observed when α becomes small and $k_l L$ becomes large in Figure 31. The second is the case where two uniform waveguides are connected without a connector. In this case, τ is a constant value determined by

$$\tau = \frac{4A_0 A_L}{(A_0 + A_L)^2} \tag{4.5}$$

and θ_t is zero. These phenomena can be observed when $k_l L \to 0$ in Figure 31.

Figure 32 shows the reflection and transmission coefficients for a bending wave incident on the connector. Similar to the case of the axial wave, the asymptotic behaviour can be explained by the two extreme cases. In the figure, it should be remembered that $k_{b,m}$ is the wavenumber of the connector determined by equation (3.19).

4.3 Comparison of exact solution with discrete models

The transmission through the connector obtained in section 3.2 is compared with approximate results obtained by the discrete model A and model B described in Appendix C. In these models the continuous non-uniform connector is modelled by discrete step-changes in area. Since the discrete model A approximates the connector as one change in area, the power transmission coefficient

$$\tau = \frac{4A_0 A_L}{(A_0 + A_L)^2} \tag{4.6}$$

is constant and the phase change in the model is only related to the length of the connector. The discrete model-B will give better result compared to discrete model-A since it adds one more uniform section.

Figures 33 and 34 show the exact transmission coefficient and the approximate transmissions obtained by the discrete models. When $k_l L \to 0$, it can be seen that the approximate results asymptote to the exact. It can also be noticed that error in the case of the bending wave is higher than that of axial wave. This is because the bending stiffness depends on the third power of the thickness. Thus when reducing the error by increasing the number

of the uniform sections, more sections will generally be required for bending motion than that for axial motion for a given accuracy.

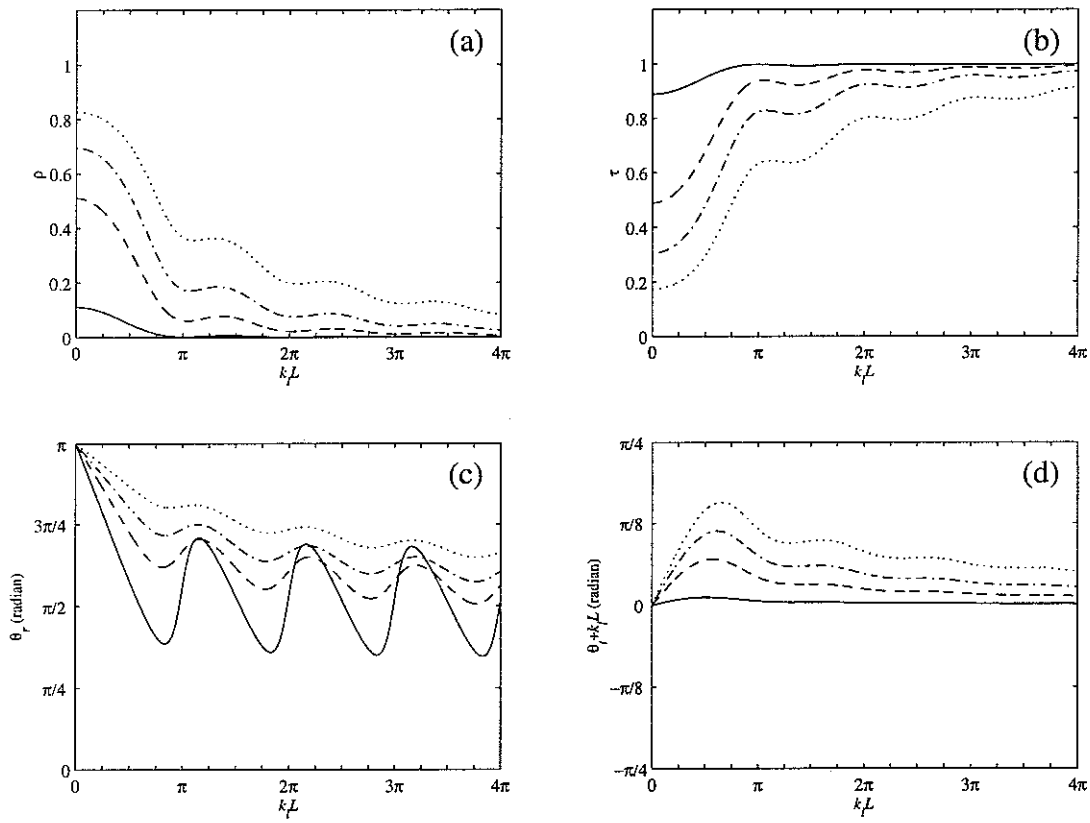

Figure 31. Reflection and transmission of an axial wave by the connector: (a) power reflection coefficient, (b) power transmission coefficient, (c) phase of the reflection coefficient, and (d) phase of the transmission coefficient multiplied by e^{ik_tL};
——— , $\alpha = 1$; ------, $\alpha = 5$; -·-·-·- , $\alpha = 10$; ····· , $\alpha = 20$.

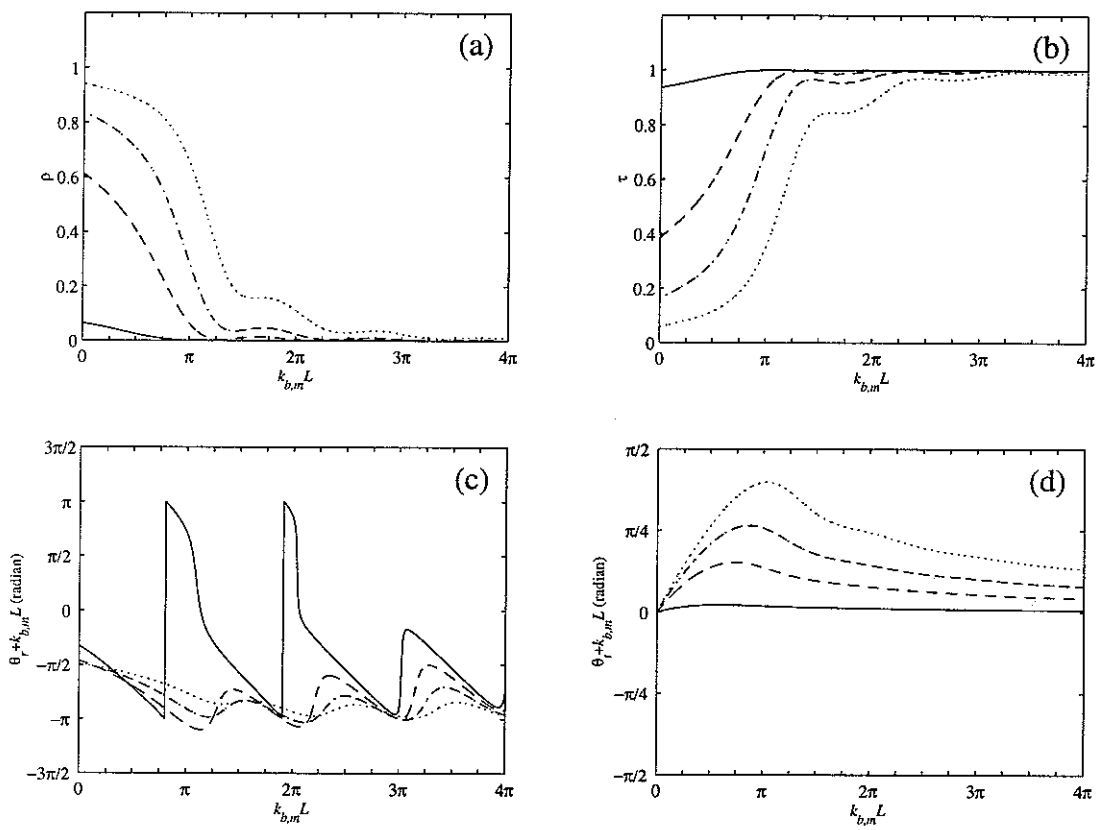

Figure 32. Reflection and transmission of a bending wave by the connector: (a) power reflection coefficient, (b) power transmission coefficient, (c) phase of $R_{T,11}$, and (d) phase of $T_{T,11}$ multiplied by $e^{ik_{b,in}L}$;

——— , $\alpha = 1$; - - - - - - , $\alpha = 5$; - · - · - · - , $\alpha = 10$; ····· , $\alpha = 20$.

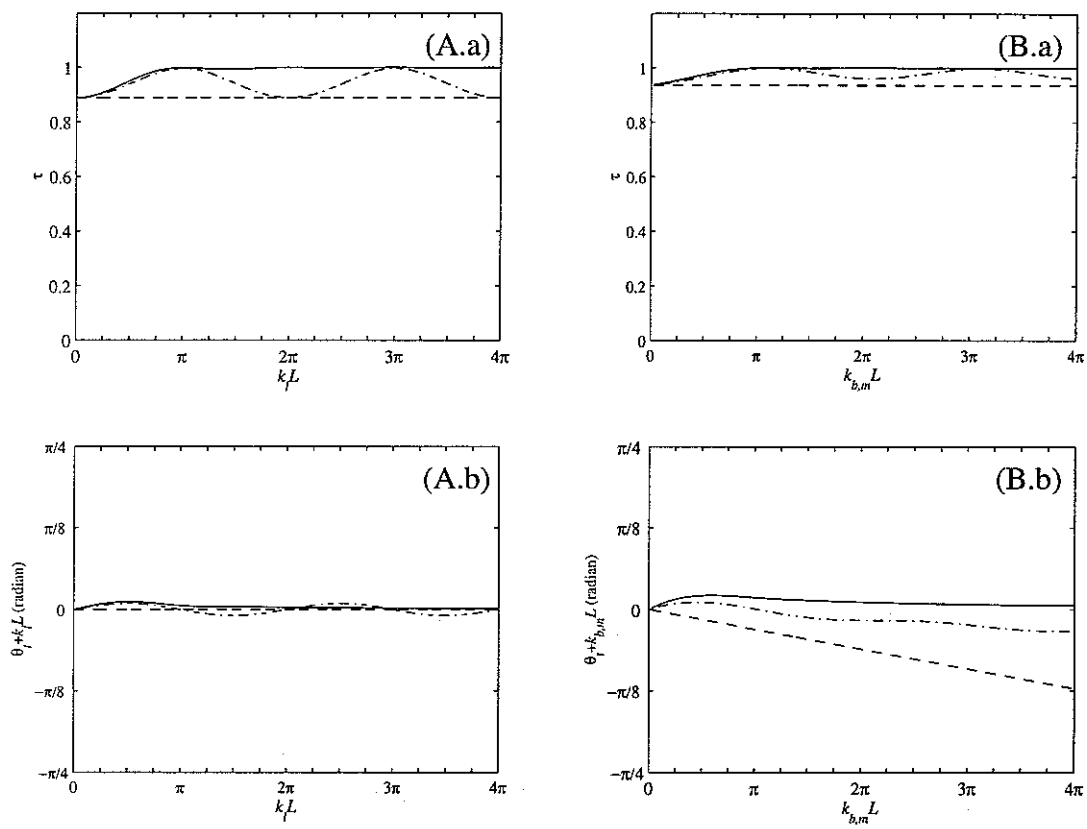

Figure 33. Exact and approximate results for the transmission through the connector with $\alpha = 1$: (A) axial wave and (B) bending wave; (a) power transmission coefficient and (b) the weighted phase of the transmission coefficient (in the case of bending wave, phase of $T_{T,11}$); ——— , exact; ------ , discrete model A; -·-·-· , discrete model B.

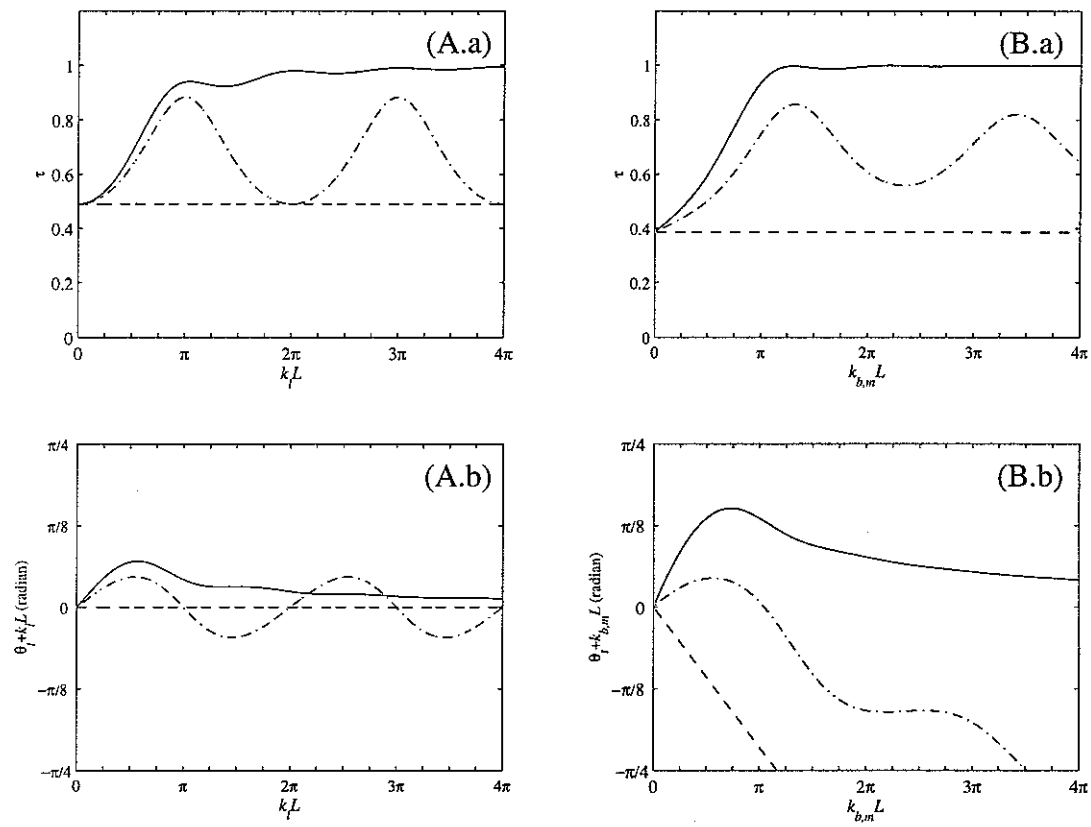

Figure 34. Exact and approximate results for the transmission through the connector with $\alpha = 5$: (A) axial wave and (B) bending wave; (a) power transmission coefficient and (b) the weighted phase of the transmission coefficient (in the case of bending wave, phase of $T_{T,11}$); ——— , exact; - - - - - - , discrete model A; -·-·-·- , discrete model B.

4.4 Summary

In this section, it was shown that the wave method developed for the non-uniform waveguide can be usefully applied to the problems related to non-uniformity. As an example, the transmission through a non-uniform connector was investigated. The result is exact and, thus, the work can be used to estimate errors occurring in using approximate methods. In section 3.3, the approximate results obtained by the discrete models were compared with the exact results obtained by this work. It was shown that as frequency increases, the error due to the discretization increases. Even though the error can be reduced by increasing the number of the uniform sections, it requires more computational power and time. These difficulties can be avoided by using the wave methods developed here.

5. CONCLUSIONS

Wave methods have been developed for the analysis of vibration of a one-dimensional non-uniform structure which has variable cross-sectional area and the second moment of area such that $A(x) \propto x^{\mu}$ and $I(x) \propto x^{\mu+2}$. The displacement, internal force and propagation matrices for axial and bending motions of the non-uniform structure were formulated in terms of waves. The reflection and transmission matrices for various conditions were also investigated. The wave methods developed in the present work can be used to predict the response of more complex, built-up structures at low computational cost.

In sections 2 and 3, axial and bending motions of a non-uniform structure were reviewed, respectively. It was shown that the axial motion can be expressed in terms of Bessel functions if the cross-sectional area of the structure varies as $A(x) \propto x^{\mu}$. This is also true of the bending motion if the geometric properties vary as $A(x) \propto x^{\mu}$ and $I(x) \propto x^{\mu+2}$. In particular, it should be noted that a rectangular structure with linearly tapered thickness and constant width satisfies the conditions. The displacement, internal force and propagation matrices at a cross section of the structure were derived by using the analytical solutions and their asymptotic behaviours were investigated. The reflection, transmission and propagation matrices for various conditions were also derived.

Throughout the work, it was shown that the non-uniformity can be considered as an additional dynamic stiffness. For example, when an end of the non-uniform bar is excited by a force, the non-uniformity of the bar makes the amplitude of the induced wave smaller than that in a uniform bar. It was shown that the influence of the non-uniformity becomes smaller as frequency increases. The effects were also seen to be different for excitation of the left- and right-hand ends, i.e. if the section decreases or increases away from the end.

The results related to bending waves were much more complicated due to the existence of the nearfield waves. Care should also be taken since bending waves are dispersive. For example, it was shown that the phase change in propagation path of length L asymptotes to $k_{b,m}L$, where $k_{b,m} = \dfrac{2k_{b,0}k_{b,L}}{k_{b,0} + k_{b,L}}$ represents the effective wavenumber of the propagation path, in the high frequency region.

In section 4, it was shown that the wave method developed for the non-uniform structure can be usefully applied to the problems involving non-uniformity. As an example, the transmission through a non-uniform connector was investigated. It was shown that the wave method can give exact results without approximation errors and at a low computational cost.

Appendix A. THE MOTION OF A STRUCTURAL WAVEGUIDE

In this appendix the wave approach to describing the motion of a structural waveguide is briefly reviewed. The aim of this work is to provide a generalized formulation of the wave approach for a waveguide where the motion can be expressed analytically. The work is developed using a uniform waveguide as a basis and is extended to the motion of a range of non-uniform waveguides.

A.1 The state of a section in terms of wave components

The amplitudes of the waves at a cross section $x=0$ of a waveguide can be grouped into two vectors, $\mathbf{a}^+$ and $\mathbf{a}^-$, in which the superscripts '+' and '−' denote the direction of propagation of the waves. Propagation in both directions can be expressed by introducing propagation matrices $\mathbf{F}^{\pm}$ such that the wave amplitudes in each direction become $\mathbf{F}^+(x)\mathbf{a}^+$ and $\mathbf{F}^-(-x)\mathbf{a}^-$ as shown in Figure A-1. The propagation matrices $\mathbf{F}^{\pm}$ are the identity matrices when $x=0$.

If generalized displacements at the section are grouped into a vector $\mathbf{w}$ and the corresponding generalized internal forces at the section into a vector, $\mathbf{f}$, the displacement and internal force vectors can then be related to the wave amplitudes by

$$\mathbf{w}=\Psi^+\mathbf{a}^+ + \Psi^-\mathbf{a}^- \tag{A.1}$$

$$\mathbf{f}=\Phi^+\mathbf{a}^+ + \Phi^-\mathbf{a}^- \tag{A.2}$$

where Ψ and Φ are the displacement and the internal force matrices, respectively. They relate the contributions that waves make to the waveguide deformation and internal forces.

For example, the propagation, displacement and internal force matrices of axial vibration of a uniform bar are given by

$$\mathbf{F}^+(x)=\left[e^{-ik_l x}\right], \qquad \mathbf{F}^-(x)=\left[e^{ik_l x}\right] \tag{A.3a,b}$$

$$\Psi^+=[1], \qquad \Psi^-=[1] \tag{A.4a,b}$$

$$\Phi^+=[\mathrm{i}EAk_l], \qquad \Phi^-=[-\mathrm{i}EAk_l] \tag{A.5a,b}$$

where k_l is the longitudinal wavenumber, E the modulus of elasticity and A the cross-sectional area of the bar. It can be noticed that, for the case of axial vibration, the relevant matrices and vectors are all composed of only a single element because only one wave component propagates in each direction.

The propagation, displacement and internal force matrices for flexural vibration of a uniform Euler-Bernoulli beam are given by

$$\mathbf{F}^{+}(x)=\begin{bmatrix} e^{-\mathrm{i}k_b x} & 0 \\ 0 & e^{-k_b x} \end{bmatrix}, \qquad \mathbf{F}^{-}(x)=\begin{bmatrix} e^{\mathrm{i}k_b x} & 0 \\ 0 & e^{k_b x} \end{bmatrix} \tag{A.6a,b}$$

$$\Psi^{+}=\begin{bmatrix} 1 & 1 \\ -\mathrm{i}k_b & -k_b \end{bmatrix}, \qquad \Psi^{-}=\begin{bmatrix} 1 & 1 \\ \mathrm{i}k_b & k_b \end{bmatrix} \tag{A.7a,b}$$

$$\Phi^{+}=EI\begin{bmatrix} \mathrm{i}k_b^{\,3} & -k_b^{\,3} \\ k_b^{\,2} & -k_b^{\,2} \end{bmatrix}, \qquad \Phi^{-}=EI\begin{bmatrix} -\mathrm{i}k_b^{\,3} & k_b^{\,3} \\ k_b^{\,2} & -k_b^{\,2} \end{bmatrix} \tag{A.8a,b}$$

where k_b is the flexural wavenumber and I the second moment of area of the beam.

The time-averaged power Π at the section is given by

$$\Pi=-\frac{1}{2}\mathrm{Re}\left\{\mathrm{i}\omega\mathbf{w}^{H}\mathbf{f}\right\} \tag{A.9}$$

where the superscript H denotes the Hermitian transpose.

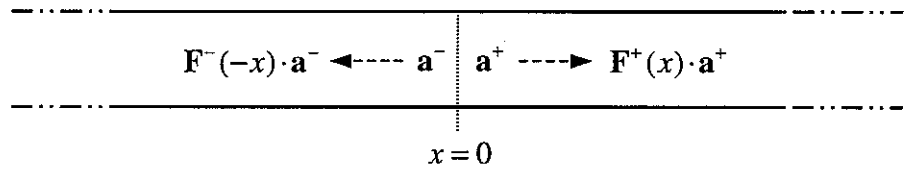

Figure A-1. Amplitudes and propagation of positive- and negative-going waves.

A.2 Wave generation by local excitation

Consider a waveguide, the left-hand end of which is excited by a local external harmonic force vector $\mathbf{f}_{ext}e^{\mathrm{i}\omega t}$, as shown in Figure A-2. Since the equilibrium condition at the end is given by

$$\Phi^{+}\mathbf{q}^{+}=\mathbf{f}_{ext} \tag{A.10}$$

the vector of the amplitudes of the induced waves, $\mathbf{q}^+$, can be written in

$$\mathbf{q}^+ = \left(\Phi^+\right)^{-1}\mathbf{f}_{ext} \tag{A.11}$$

Similarly, if the right-hand end of a waveguide is excited by a local external harmonic force vector $\mathbf{f}_{ext}e^{i\omega t}$ as shown in Figure A-3, the vector of the amplitudes of the induced waves, $\mathbf{q}^-$, can be written in

$$\mathbf{q}^- = -\left(\Phi^-\right)^{-1}\mathbf{f}_{ext} \tag{A.12}$$

Consider an infinite waveguide, a cross section of which is excited by a local external harmonic force vector $\mathbf{f}_{ext}e^{i\omega t}$, as shown in Figure A-4. Since continuity and equilibrium conditions at the section are given by

$$\Psi^+\mathbf{q}^+ = \Psi^-\mathbf{q}^- \tag{A.13}$$

$$\Phi^+\mathbf{q}^+ - \Phi^-\mathbf{q}^- = \mathbf{f}_{ext} \tag{A.14}$$

where now $\mathbf{q}^{\pm}$ are wave amplitudes at either side of the excited cross-section, the vectors $\mathbf{q}^+$ and $\mathbf{q}^-$ are given by

$$\mathbf{q}^+ = \left[\Phi^+ - \Phi^-\left(\Psi^-\right)^{-1}\Psi^+\right]^{-1}\mathbf{f}_{ext} \tag{A.15}$$

$$\mathbf{q}^- = \left[\Phi^+\left(\Psi^+\right)^{-1}\Psi^- - \Phi^-\right]^{-1}\mathbf{f}_{ext} \tag{A.16}$$

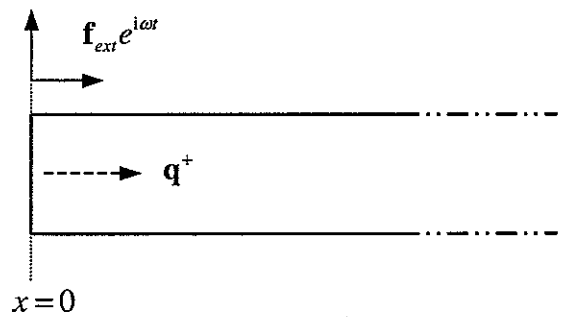

Figure A-2. A waveguide, the left-hand end of which is excited by local external forces.

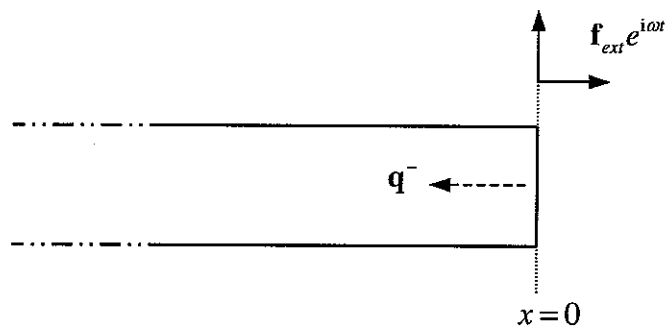

Figure A-3. A waveguide, the right-hand end of which is excited by local external forces.

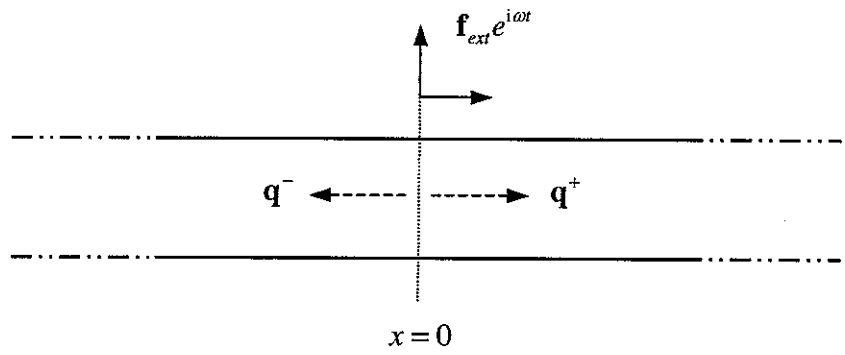

Figure A-4. A waveguide, a section of which is excited by local external forces.

A.3 Reflection at boundaries

If waves with amplitudes $\mathbf{a}^+$ are incident upon the right-hand end of a waveguide as shown in Figure A-5, the amplitudes of the reflected waves, $\mathbf{a}^-$, can be expressed such that

$$\mathbf{a}^- = \mathbf{R}\mathbf{a}^+ \tag{A.17}$$

where $\mathbf{R}$, the reflection matrix of the boundary, is determined by the boundary conditions at the end. If the boundary condition is expressed by a local dynamic stiffness matrix $\mathbf{K}$ such that

$$\mathbf{f} = \mathbf{K}\mathbf{w} \tag{A.18}$$

combining equation (A.18) with equations (A.1) and (A.2) gives

$$\Phi^+\mathbf{a}^+ + \Phi^-\mathbf{a}^- = \mathbf{K}\left(\Psi^+\mathbf{a}^+ + \Psi^-\mathbf{a}^-\right) \tag{A.19}$$

Thus substituting equation (A.17) in equation (A.19) gives

$$\mathbf{R} = -\left(\mathbf{K}\Psi^{-} - \Phi^{-}\right)^{-1}\left(\mathbf{K}\Psi^{+} - \Phi^{+}\right) \tag{A.20}$$

It should be noticed that, if waves are incident upon the left-hand end of the waveguide, the reflection matrix is the same as equation (A.20) but with the superscripts in equation (A.20) reversed. Even though equation (A.20) is simple, it cannot be used in some situations where $\mathbf{K}$ does not exist - for example, a simply supported end of a beam. The numerical difficulty can be avoided by using an alternative form [24].

If translational and rotational dynamic stiffnesses $\bar{K}_T$ and $\bar{K}_R$ are attached at a end of a uniform Euler-Bernoulli beam, the stiffness matrix is given by

$$\mathbf{K} = \begin{bmatrix} \bar{K}_T & 0 \\ 0 & \bar{K}_R \end{bmatrix} \tag{A.21}$$

and the reflection matrix $\mathbf{R}$ at the end is found to be [23]

$$\mathbf{R} = \begin{bmatrix} 1-\mathrm{i}K_T & \mathrm{i}(1-K_T) \\ -1+\mathrm{i}K_R & 1+K_R \end{bmatrix}^{-1} \begin{bmatrix} 1+\mathrm{i}K_T & \mathrm{i}(1+K_T) \\ 1+\mathrm{i}K_R & -1+K_R \end{bmatrix} \tag{A.22}$$

where dimensionless stiffnesses $K_T = \bar{K}_T / EIk_b^3$ and $K_R = \bar{K}_R / EIk_b$ have been introduced.

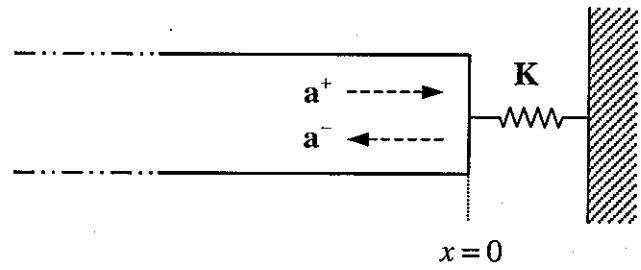

Figure A-5. Wave reflection at an end with generalized dynamic stiffness.

A.4 Reflection and transmission at a discontinuity

Consider waves with amplitudes $\mathbf{a}^{+}$ incident upon a discontinuity at a section of a waveguide. The discontinuity may be an external impedance-mismatching component attached to the section of an infinite waveguide, or a junction between two semi-infinite waveguides, or combination of both cases as shown in Figure A-6. Amplitudes of reflected and transmitted waves, $\mathbf{a}^{-}$ and $\mathbf{b}^{+}$, can then be expressed as

$$\mathbf{a}^- = \mathbf{R}\mathbf{a}^+ \tag{A.23}$$

$$\mathbf{b}^+ = \mathbf{T}\mathbf{a}^+ \tag{A.24}$$

where $\mathbf{R}$ is the reflection matrix of the discontinuity and $\mathbf{T}$ is the transmission matrix. Since the continuity and equilibrium conditions at the discontinuity are given by

$$\mathbf{w}_a = \mathbf{w}_b \tag{A.25}$$

$$\mathbf{f}_a - \mathbf{f}_b = \mathbf{K}\mathbf{w}_a \tag{A.26}$$

combining equations (A.25) and (A.26) with equations (A.1) and (A.2) gives

$$\Psi_a^{\ +}\mathbf{a}^+ + \Psi_a^{\ -}\mathbf{a}^- = \Psi_b^{\ +}\mathbf{b}^+ \tag{A.27}$$

$$\Phi_a^{\ +}\mathbf{a}^+ + \Phi_a^{\ -}\mathbf{a}^- - \Phi_b^{\ +}\mathbf{b}^+ = \mathbf{K}\Psi_b^{\ +}\mathbf{b}^+ \tag{A.28}$$

Thus combining equations (A.27) and (A.28) with equations (A.23) and (A.24) gives

$$\mathbf{R} = -\left[\mathbf{K}\Psi_a^{\ -} + \Phi_b^{\ +}\left(\Psi_b^{\ +}\right)^{-1}\Psi_a^{\ -} - \Phi_a^{\ -}\right]^{-1}\left[\mathbf{K}\Psi_a^{\ +} + \Phi_b^{\ +}\left(\Psi_b^{\ +}\right)^{-1}\Psi_a^{\ +} - \Phi_a^{\ +}\right] \tag{A.29}$$

$$\mathbf{T} = \left[\mathbf{K}\Psi_b^{\ +} - \Phi_a^{\ -}\left(\Psi_a^{\ -}\right)^{-1}\Psi_b^{\ +} + \Phi_b^{\ +}\right]^{-1}\left[-\Phi_a^{\ -}\left(\Psi_a^{\ -}\right)^{-1}\Psi_a^{\ +} + \Phi_a^{\ +}\right] \tag{A.30}$$

Even though equations (A.29) and (A.30) are simple, they cannot be used in some situations where $\mathbf{K}$ does not exist as discussed above - for example, a simply supported section of a beam. The numerical difficulty can be avoided by using an alternative form [24].

If two uniform and semi-infinite beams are connected together, and there is no external impedance attached to the junction, the reflection and transmission matrices are given by [23]

$$\mathbf{R} = \frac{2}{\Delta}\begin{bmatrix} -2(\beta^2-1)\gamma - \mathrm{i}\beta(1-\gamma)^2 & (1+\mathrm{i})\beta(1-\gamma^2) \\ (1-\mathrm{i})\beta(1-\gamma^2) & -2(\beta^2-1)\gamma + \mathrm{i}\beta(1-\gamma)^2 \end{bmatrix},$$
$$\mathbf{T} = \frac{4}{\Delta}\begin{bmatrix} (1+\beta)(1+\gamma) & -(1-\mathrm{i}\beta)(1-\gamma) \\ -(1+\mathrm{i}\beta)(1-\gamma) & (1+\beta)(1+\gamma) \end{bmatrix} \tag{A.31a, b}$$

where $\Delta = (1+\beta)^2(1+\gamma)^2 - (1+\beta^2)(1-\gamma)^2$, $\beta = k_{b,2}/k_{b,1}$ and $\gamma = (EIk_b^{\ 2})_2/(EIk_b^{\ 2})_1$. It should be noted that the transmission and reflection matrices are independent of frequency in this case.

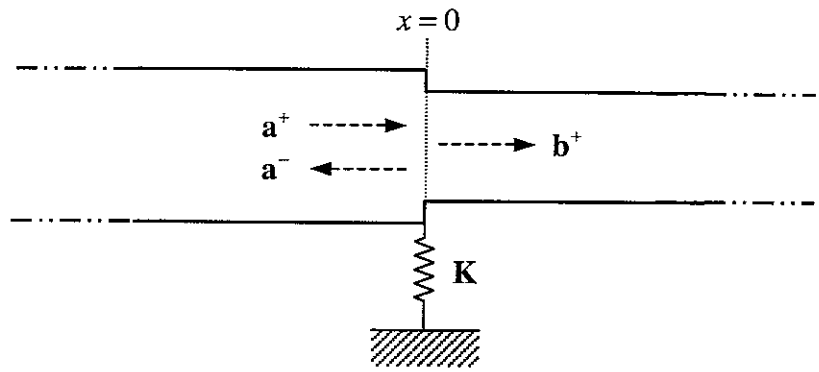

Figure A-6. Wave reflection and transmission at a discontinuity.

Appendix B. BESSEL FUNCTIONS

In this appendix various properties of Bessel functions are summarized. They relate to various forms of Bessel's equation and their solutions, the recurrence relations of Bessel functions, the properties of Bessel functions of half-integral order and asymptotic behaviour. Further details can be found in [3, 26, 27].

B.1 Bessel's equation

A differential equation of the form

$$\frac{d^2\psi}{dz^2}+\frac{1}{z}\frac{d\psi}{dz}+\left(1-\frac{\nu^2}{z^2}\right)\psi=0 \tag{B.1}$$

where ν is a non-negative real number, is known as Bessel's equation of order ν. Its solutions are denoted by $J_\nu(z)$, the Bessel function of the first kind of order ν, and $Y_\nu(z)$, the Bessel function of the second kind of order ν. The complete solution of Bessel's equation can be written as a linear combination of $J_\nu(z)$ and $Y_\nu(z)$.

The complete solution can also be written in the form

$$\psi=C_1H_\nu^{(1)}(z)+C_2H_\nu^{(2)}(z) \tag{B.2}$$

where C_1 and C_2 represent arbitrary constants, and $H_\nu^{(1)}(z)$ and $H_\nu^{(2)}(z)$ are Bessel functions of the third kind of order ν and are defined by

$$H_\nu^{(1)}(z)=J_\nu(z)+\mathrm{i}Y_\nu(z) \tag{B.3}$$

$$H_\nu^{(2)}(z)=J_\nu(z)-\mathrm{i}Y_\nu(z) \tag{B.4}$$

$H_\nu^{(1,2)}(z)$ are also named the Hankel functions of the first and second kinds and represent waves travelling in the negative and positive z-directions, respectively.

A differential equation of the form

$$\frac{d^2\psi}{dz^2}+\frac{1}{z}\frac{d\psi}{dz}-\left(1+\frac{\nu^2}{z^2}\right)\psi=0 \tag{B.5}$$

is called the modified Bessel's equation of order v. Its solutions, termed the modified Bessel functions, are denoted by $I_v(z)$ and $K_v(z)$ and the complete solution can be written in the form

$$\psi = C_1 I_v(z) + C_2 K_v(z) \tag{B.6}$$

Figure B-1 shows $J_v(z)$, $Y_v(z)$, $I_v(z)$ and $K_v(z)$ for several orders v. Bessel's equations (B.1) and (B.5) has a regular singular point at $z = 0$ [28]. This singularity may cause numerical difficulties in the evaluation of Bessel functions near $z = 0$.

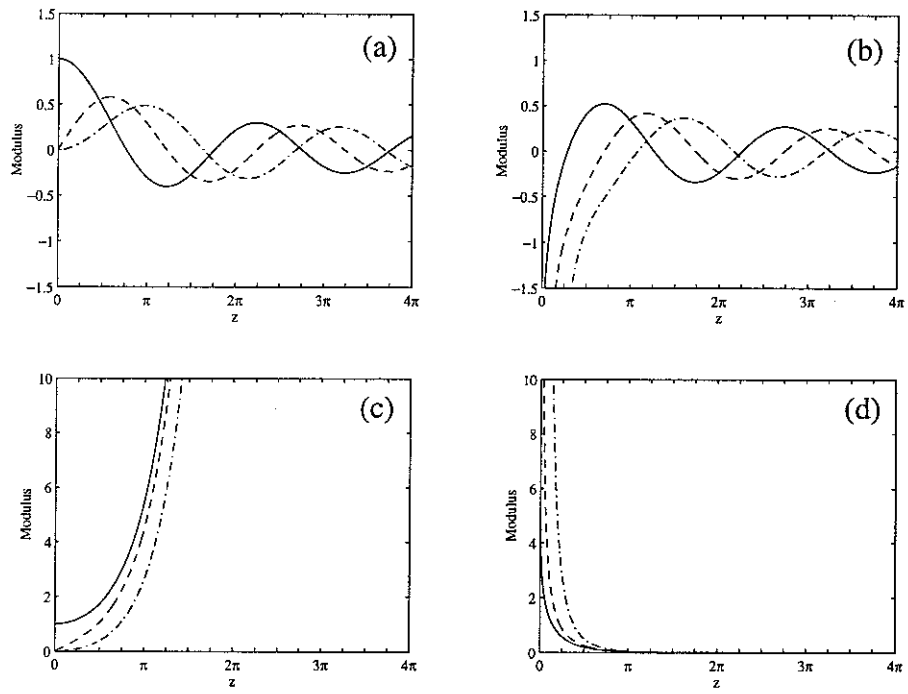

Figure B-1. Bessel functions: (a) $J_v(z)$, (b) $Y_v(z)$, (c) $I_v(z)$ and (d) $K_v(z)$;
——, $v = 0$; ------, $v = 1$; -·-·-·-, $v = 2$.

B.2 Alternative forms of Bessel's equation

Many differential equations are transformable into Bessel's equation. One of the very useful general forms is [29]

$$z^2 \frac{d^2\psi}{dz^2} + (1+2\alpha) z \frac{d\psi}{dz} + (\beta^2 z^{2\gamma} + \delta^2)\psi = 0 \tag{B.7}$$

the solution of which is given by

$$\psi = z^{-\alpha}\left[C_1 H_\nu^{(1)}\left(\frac{\beta z^\gamma}{\gamma}\right) + C_2 H_\nu^{(2)}\left(\frac{\beta z^\gamma}{\gamma}\right)\right] \tag{B.8}$$

where

$$\nu = \frac{\sqrt{\alpha^2 - \delta^2}}{\gamma} \tag{B.9}$$

Similarly, the general form of the differential equation for the modified Bessel functions is

$$z^2\frac{d^2\psi}{dz^2} + (1+2\alpha)z\frac{d\psi}{dz} + (-\beta^2 z^{2\gamma} + \delta^2)\psi = 0 \tag{B.10}$$

the solution of which is given by

$$\psi = z^{-\alpha}\left\{C_1 I_\nu\left(\frac{\beta z^\gamma}{\gamma}\right) + C_2 K_\nu\left(\frac{\beta z^\gamma}{\gamma}\right)\right\} \tag{B.11}$$

Several alternative forms of Bessel's equation and their solutions are

$$\frac{d^2\psi}{dz^2} + \frac{(1+2\nu)}{z}\frac{d\psi}{dz} + k^2\psi = 0, \qquad \psi = z^{-\nu}\left\{C_1 H_\nu^{(1)}(kz) + C_2 H_\nu^{(2)}(kz)\right\} \tag{B.12a, b}$$

$$z\frac{d^2\psi}{dz^2} + (1+\nu)\frac{d\psi}{dz} + k^2\psi = 0, \qquad \psi = z^{-\nu/2}\left\{C_1 H_\nu^{(1)}\left(2k\sqrt{z}\right) + C_2 H_\nu^{(2)}\left(2k\sqrt{z}\right)\right\} \tag{B.13a, b}$$

and

$$z\frac{d^2\psi}{dz^2} + (1+\nu)\frac{d\psi}{dz} - k^2\psi = 0, \qquad \psi = z^{-\nu/2}\left\{C_1 I_\nu\left(2k\sqrt{z}\right) + C_2 K_\nu\left(2k\sqrt{z}\right)\right\} \tag{B.14a, b}$$

If equations (B.13a) and (B.14a) are combined as

$$\left[z\frac{d^2}{dz^2} + (1+\nu)\frac{d}{dz} + k^2\right]\left[z\frac{d^2}{dz^2} + (1+\nu)\frac{d}{dz} - k^2\right]\psi = 0 \tag{B.15}$$

and expanded, the differential equation of 4th order

$$z^2\frac{d^4\psi}{dz^4} + 2(2+\nu)z\frac{d^3\psi}{dz^3} + (1+\nu)(2+\nu)\frac{d^2\psi}{dz^2} - k^4\psi = 0 \tag{B.16}$$

can be obtained. The general solution of equation (B.16) can be written as

$$\psi = z^{-\nu/2}\left[C_1 H_\nu^{(1)}\left(2k\sqrt{z}\right) + C_2 H_\nu^{(2)}\left(2k\sqrt{z}\right) + C_3 I_\nu\left(2k\sqrt{z}\right) + C_4 K_\nu\left(2k\sqrt{z}\right)\right] \tag{B.17}$$

B.3 Recurrence relations

The Bessel function of the first kind, $J_\nu(z)$, satisfies

$$\frac{d}{dz}\left[z^\nu J_\nu(z)\right]=z^\nu J_{\nu-1}(z) \tag{B.18}$$

and

$$\frac{d}{dz}\left[z^{-\nu} J_\nu(z)\right]=-z^{-\nu} J_{\nu+1}(z) \tag{B.19}$$

When the derivatives appearing in equations (B.18) and (B.19) are expanded (where $()'$ denotes $\frac{d}{dz}$) and the results are simplified, equations

$$zJ'_\nu(z)+\nu J_\nu(z)=zJ_{\nu-1}(z) \tag{B.20}$$

and

$$zJ'_\nu(z)-\nu J_\nu(z)=-zJ_{\nu+1}(z) \tag{B.21}$$

are obtained. Subtracting (B.21) from (B.20) gives

$$J_{\nu+1}(z)=\frac{2\nu}{z}J_\nu(z)-J_{\nu-1}(z) \tag{B.22}$$

and adding (B.20) to (B.21) gives

$$J'_\nu(z)=\frac{1}{2}\left\{J_{\nu-1}(z)-J_{\nu+1}(z)\right\} \tag{B.23}$$

Equations (B.18) to (B.23) are called the recurrence relations of Bessel functions and also hold for the functions $Y_\nu(z)$, $H_\nu^{(1)}(z)$ and $H_\nu^{(2)}(z)$.

Similarly, the recurrence formulas of the modified Bessel functions are summarized as

$$\frac{d}{dz}\left[z^\nu I_\nu(z)\right]=z^\nu I_{\nu-1}(z) \tag{B.24}$$

$$\frac{d}{dz}\left[z^{-\nu} I_\nu(z)\right]=z^{-\nu} I_{\nu+1}(z) \tag{B.25}$$

$$zI'_\nu(z)+\nu I_\nu(z)=zI_{\nu-1}(z) \tag{B.26}$$

$$zI'_\nu(z)-\nu I_\nu(z)=zI_{\nu+1}(z) \tag{B.27}$$

$$I_{\nu+1}(z) = -\frac{2\nu}{z} I_\nu(z) + I_{\nu-1}(z) \tag{B.28}$$

$$I'_\nu(z) = \frac{1}{2}\{I_{\nu-1}(z) + I_{\nu+1}(z)\} \tag{B.29}$$

and

$$\frac{d}{dz}\left[z^\nu K_\nu(z)\right] = -z^\nu K_{\nu-1}(z) \tag{B.30}$$

$$\frac{d}{dz}\left[z^{-\nu} K_\nu(z)\right] = -z^{-\nu} K_{\nu+1}(z) \tag{B.31}$$

$$zK'_\nu(z) + \nu K_\nu(z) = -zK_{\nu-1}(z) \tag{B.32}$$

$$zK'_\nu(z) - \nu K_\nu(z) = -zK_{\nu+1}(z) \tag{B.33}$$

$$K_{\nu+1}(z) = \frac{2\nu}{z} K_\nu(z) + K_{\nu-1}(z) \tag{B.34}$$

$$K'_\nu(z) = -\frac{1}{2}\{K_{\nu-1}(z) + K_{\nu+1}(z)\} \tag{B.35}$$

B.4 Bessel functions of half-integral order

Bessel function of half-integral order $n+\frac{1}{2}$, where n is an integer, can be expressed in closed form in terms of elementary functions. For instance, Bessel functions of order $\pm\frac{1}{2}$ can be expressed as

$$J_{1/2}(z) = \sqrt{\frac{2}{\pi z}} \sin z = Y_{-1/2}(z) \tag{B.36a, b}$$

and

$$J_{-1/2}(z) = \sqrt{\frac{2}{\pi z}} \cos z = -Y_{1/2}(z) \tag{B.37a, b}$$

Now, from (B.22), it follows that

$$J_{3/2}(z)=\frac{1}{z}J_{1/2}(z)-J_{-1/2}(z),$$
$$=\sqrt{\frac{2}{\pi z}}\left(\frac{1}{z}\sin z-\cos z\right) \qquad \text{(B.38a, b)}$$

$$Y_{3/2}(z)=\frac{1}{z}Y_{1/2}(z)-Y_{-1/2}(z),$$
$$=-\sqrt{\frac{2}{\pi z}}\left(\frac{1}{z}\cos z+\sin z\right) \qquad \text{(B.39a, b)}$$

$$J_{5/2}(z)=\sqrt{\frac{2}{\pi z}}\left\{\left(\frac{3}{z^2}-1\right)\sin z-\frac{3}{z}\cos z\right\} \qquad \text{(B.40)}$$

$$Y_{5/2}(z)=-\sqrt{\frac{2}{\pi z}}\left\{\left(\frac{3}{z^2}-1\right)\cos z+\frac{3}{z}\sin z\right\} \qquad \text{(B.41)}$$

and so on.

By using equations (B.36) to (B.39), the Hankel functions can be written in the form

$$H_{1/2}^{(1)}(z)=-\mathrm{i}\sqrt{\frac{2}{\pi z}}e^{\mathrm{i}z}=-\mathrm{i}H_{-1/2}^{(1)}(z) \qquad \text{(B.42a, b)}$$

$$H_{1/2}^{(2)}(z)=\mathrm{i}\sqrt{\frac{2}{\pi z}}e^{-\mathrm{i}z}=\mathrm{i}H_{-1/2}^{(2)}(z) \qquad \text{(B.43a, b)}$$

$$H_{3/2}^{(1)}(z)=-\sqrt{\frac{2}{\pi z}}\left(1+\frac{\mathrm{i}}{z}\right)e^{\mathrm{i}z} \qquad \text{(B.44)}$$

$$H_{3/2}^{(2)}(z)=-\sqrt{\frac{2}{\pi z}}\left(1-\frac{\mathrm{i}}{z}\right)e^{-\mathrm{i}z} \qquad \text{(B.45)}$$

$$H_{5/2}^{(1)}(z)=-\sqrt{\frac{2}{\pi z}}\left\{\frac{3}{z}+\mathrm{i}\left(\frac{3}{z^2}-1\right)\right\}e^{\mathrm{i}z} \qquad \text{(B.46)}$$

$$H_{5/2}^{(2)}(z)=-\sqrt{\frac{2}{\pi z}}\left\{\frac{3}{z}-\mathrm{i}\left(\frac{3}{z^2}-1\right)\right\}e^{-\mathrm{i}z} \qquad \text{(B.47)}$$

The modified Bessel functions of half-integral order $n+\frac{1}{2}$ can also be written in the form

$$I_{1/2}(z)=\sqrt{\frac{2}{\pi z}}\sinh z \tag{B.48}$$

$$K_{1/2}(z)=\sqrt{\frac{\pi}{2z}}e^{-z}=K_{-1/2}(z) \tag{B.49}$$

$$I_{3/2}(z)=\sqrt{\frac{2}{\pi z}}\left(\cosh z-\frac{1}{z}\sinh z\right) \tag{B.50}$$

$$K_{3/2}(z)=\sqrt{\frac{\pi}{2z}}\left(1+\frac{1}{z}\right)e^{-z} \tag{B.51}$$

$$I_{5/2}(z)=\sqrt{\frac{2}{\pi z}}\left\{\left(\frac{3}{z^2}+1\right)\sinh z-\frac{3}{z}\cosh z\right\} \tag{B.52}$$

$$K_{5/2}(z)=\sqrt{\frac{\pi}{2z}}\left(\frac{3}{z^2}+\frac{3}{z}+1\right)e^{-z} \tag{B.53}$$

and so on.

B.5 Limiting behaviour for large argument

When $|z|\gg 1, |z|\gg|\nu|^2$ and $-\frac{\pi}{2}\le \text{phase}(z)\le\frac{\pi}{2}$, [3]

$$H_\nu^{(1)}(z)=\sqrt{\frac{2}{\pi z}}e^{\mathrm{i}\left(z-\frac{1}{4}\pi-\frac{1}{2}\nu\pi\right)}\left\{1-\frac{4\nu^2-1^2}{1!(\mathrm{i}8z)}+\frac{(4\nu^2-1^2)(4\nu^2-3^2)}{2!(\mathrm{i}8z)^2}-\ldots\right\} \tag{B.54}$$

$$H_\nu^{(2)}(z)=\sqrt{\frac{2}{\pi z}}e^{-\mathrm{i}\left(z-\frac{1}{4}\pi-\frac{1}{2}\nu\pi\right)}\left\{1+\frac{4\nu^2-1^2}{1!(\mathrm{i}8z)}+\frac{(4\nu^2-1^2)(4\nu^2-3^2)}{2!(\mathrm{i}8z)^2}+\ldots\right\} \tag{B.55}$$

If the terms higher than the first term in the series in equations (B.54) and (B.55) can be neglected, the Hankel functions asymptote to

$$H_\nu^{(1)}(z)\approx\sqrt{\frac{2}{\pi z}}e^{\mathrm{i}\left(z-\frac{1}{4}\pi-\frac{1}{2}\nu\pi\right)},\qquad H_\nu^{(2)}(z)\approx\sqrt{\frac{2}{\pi z}}e^{-\mathrm{i}\left(z-\frac{1}{4}\pi-\frac{1}{2}\nu\pi\right)} \tag{B.56a, b}$$

Thus it follows that

$$\frac{H_{\nu+1}^{(1)}(z)}{H_\nu^{(1)}(z)}\approx-\mathrm{i},\qquad \frac{H_{\nu+1}^{(2)}(z)}{H_\nu^{(2)}(z)}\approx\mathrm{i} \tag{B.57a, b}$$

and

$$\frac{H_{\nu+2}^{(1)}(z)}{H_{\nu}^{(1)}(z)} \approx -1, \qquad \frac{H_{\nu+2}^{(2)}(z)}{H_{\nu}^{(2)}(z)} \approx -1 \tag{B.58a, b}$$

When $|z| \gg 1, |z| \gg |\nu|^2$ and $0 \le \text{phase}(z) \le \pi$ [3],

$$\begin{aligned} I_{\nu}(z) = & \frac{e^{z}}{\sqrt{2\pi z}}\left\{1 - \frac{4\nu^2 - 1^2}{1!(8z)} + \frac{(4\nu^2 - 1^2)(4\nu^2 - 3^2)}{2!(8z)^2} - \ldots\right\} \\ & + e^{i\left(\nu+\frac{1}{2}\right)\pi}\frac{e^{-z}}{\sqrt{2\pi z}}\left\{1 + \frac{4\nu^2 - 1^2}{1!(8z)} + \frac{(4\nu^2 - 1^2)(4\nu^2 - 3^2)}{2!(8z)^2} + \ldots\right\} \end{aligned} \tag{B.59}$$

while, for $-\pi < \text{phase}(z) \le 0$,

$$\begin{aligned} I_{\nu}(z) = & \frac{e^{z}}{\sqrt{2\pi z}}\left\{1 - \frac{(4\nu^2 - 1^2)}{1!(8z)} + \frac{(4\nu^2 - 1^2)(4\nu^2 - 3^2)}{2!(8z)^2} - \ldots\right\} \\ & + e^{-i\left(\nu+\frac{1}{2}\right)\pi}\frac{e^{-z}}{\sqrt{2\pi z}}\left\{1 + \frac{(4\nu^2 - 1^2)}{1!(8z)} + \frac{(4\nu^2 - 1^2)(4\nu^2 - 3^2)}{2!(8z)^2} + \ldots\right\} \end{aligned} \tag{B.60}$$

If the real part of z is positive, the second series in equations (B.59) and (B.60) can be neglected and $I_{\nu}(z)$ asymptotes to

$$I_{\nu}(z) \approx \frac{e^{z}}{\sqrt{2\pi z}} \tag{B.61}$$

Thus it follows that

$$\frac{I_{\nu+1}(z)}{I_{\nu}(z)} \approx 1, \qquad \frac{I_{\nu+2}(z)}{I_{\nu}(z)} \approx 1 \tag{B.62a, b}$$

Finally, when $|z| \gg 1, |z| \gg |\nu|^2$ and $-\pi < \text{phase}(z) \le \pi$ [3],

$$K_{\nu}(z) = \sqrt{\frac{\pi}{2z}}e^{-z}\left\{1 + \frac{(4\nu^2 - 1^2)}{1!(8z)} + \frac{(4\nu^2 - 1^2)(4\nu^2 - 3^2)}{2!(8z)^2} + \ldots\right\} \tag{B.63}$$

If the terms higher than the first term in the series in equations (B.63) can be neglected, $K_{\nu}(z)$ asymptotes to

$$K_{\nu}(z) \approx \sqrt{\frac{\pi}{2z}}e^{-z} \tag{B.64}$$

and it follows that

$$\frac{K_{\nu+1}(z)}{K_{\nu}(z)} \approx 1, \qquad \frac{K_{\nu+2}(z)}{K_{\nu}(z)} \approx 1 \tag{B.65a, b}$$

Appendix C. NUMERICAL CONSIDERATIONS

In this appendix various numerical aspects of the wave approach are briefly reviewed. They relate to the effect of discretization, accuracy etc. They are illustrated with regard to wave transmission through the structure shown in Figure C-1.

Consider two semi-infinite cylindrical bars which are connected as shown in Figure C-1. Here $\mathbf{a}^+$, $\mathbf{a}^-$ and $\mathbf{d}^+$ refer to amplitude vectors of incident, reflected and transmitted waves, respectively. In this case, the connector between two bars has conical variation in cross-sectional area such that

$$A = A_0\left(1+\alpha\frac{x}{L}\right)^2 \tag{C.1}$$

For simplicity, the two bars and the connector are assumed to all have same material properties.

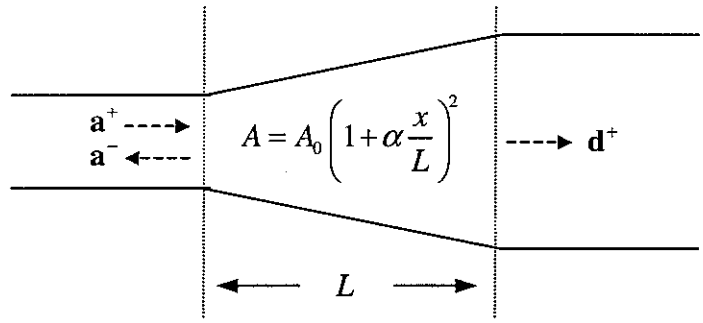

Figure C-1. Connector with conical area change.

C.1 Exact solution

As described in [25], $\mathbf{d}^+$ can be expressed exactly in terms of $\mathbf{a}^+$ such that

$$\mathbf{d}^+ = e^{-ik_lL}\left[(1+\alpha)+\frac{\alpha^2}{4k_l^2L^2}\left\{1-i2k_lL-e^{-i2k_lL}\right\}\right]^{-1}\mathbf{a}^+ \tag{C.2}$$

If the exponential term in the bracket in equation (C.2) is expanded such that

$$e^{-i2k_lL} = 1-i2k_lL+\frac{(-i2k_lL)^2}{2!}+\frac{(-i2k_lL)^3}{3!}+\ldots \tag{C.3}$$

then

$$\begin{aligned}\mathbf{d}^{+} &= e^{-ik_l L}\left[(1+\alpha)+\frac{\alpha^2}{4k_l{}^2L^2}\left\{2(k_lL)^2-i\frac{4}{3}(k_lL)^3+\ldots\right\}\right]^{-1}\mathbf{a}^{+} \\ &= e^{-ik_l L}\left[\left(1+\alpha+\frac{\alpha^2}{2}\right)-ik_lL\frac{\alpha^2}{3}+\ldots\right]^{-1}\mathbf{a}^{+} \\ &= e^{-ik_l L}\left[\frac{A_0+A_L}{2A_0}-ik_lL\frac{\alpha^2}{3}+\ldots\right]^{-1}\mathbf{a}^{+}\end{aligned} \qquad \text{(C.4a, b, c)}$$

where A_L is cross-sectional area at $x=L$ and it is noted that

$$A_L = A_0(1+\alpha)^2 \qquad \text{(C.5)}$$

When $k_lL \ll 1$, the terms from the second term in the bracket in equation (C.4c) can be neglected, then

$$\mathbf{d}^{+} \approx e^{-ik_l L}\left(\frac{A_0+A_L}{2A_0}\right)^{-1}\mathbf{a}^{+} \qquad \text{(C.6)}$$

The power transmission coefficient τ in this case is given by [25]

$$\tau = \frac{A_L}{A_0}\left|\frac{\mathbf{d}^{+}}{\mathbf{a}^{+}}\right|^2 \qquad \text{(C.7)}$$

Thus combining equations (C.7) with (C.6) shows that τ asymptotes to

$$\tau \approx \frac{4A_0A_L}{(A_0+A_L)^2} \qquad \text{(C.8)}$$

Equations (C.6) and (C.8) indicate that the existence of the connector can be neglected when the frequency is very low and the connection length is very short.

When $k_lL \gg 1$, the second terms in the bracket in equation (C.2) can be neglected, then

$$\mathbf{d}^{+} \approx e^{-ik_l L}(1+\alpha)^{-1}\mathbf{a}^{+} \qquad \text{(C.9)}$$

Thus combining equations (C.7) with (C.9) shows that

$$\tau \approx 1 \qquad \text{(C.10)}$$

Equation (C.10) indicates that waves incident on the connector are transmitted without reflection if the non-uniformity per unit length is small as discussed by Lighthill [30].

C.2 Discrete models

When the connector is assumed to be composed of many small uniform sections, it is possible to analyse motion of the connector with a discrete wave model as described in [25]. There are many possible different discrete models depending on how it is chosen to divide the connector into small sections. Among the models, the two models shown in Figures C-2 and C-3, which seem to be used most intuitively, are discussed here. In the first, the connector is simply considered as one area change. In the second, the connector is divided into three sections in which the cross-sectional area of the middle section, A_m, is determined by

$$A_m = \frac{A_0 + A_L}{2} \tag{C.11}$$

For the discrete model A, $\mathbf{d}^+$ is given by

$$\mathbf{d}_A{}^+ = e^{-ik_l L}\left[\frac{A_0 + A_L}{2A_0}\right]^{-1}\mathbf{a}^+ \tag{C.12}$$

When equations (C.4c) and (C.12) are compared, it can be seen that the errors in $\mathbf{d}_A{}^+$ depend on the length of the non-uniformity through $k_l L$ and the degree of non-uniformity through α. It can be noted that, when $k_l L \ll 1$ and thus the terms higher than the second term in the bracket in equation (C.4c), the errors in the phase of $\mathbf{d}_A{}^+$ are proportional to $k_l L$ while the errors in the amplitude of $\mathbf{d}_A{}^+$ are proportional to $(k_l L)^2$. Thus the power transmission coefficient might be more accurately predicted than the response when $k_l L \ll 1$.

For the discrete model B,

$$\mathbf{d}_B{}^+ = e^{-ik_l L}\left[\frac{(A_0 + A_m)(A_m + A_L)}{4A_0 A_m} + \frac{(A_m - A_0)(A_L - A_0)}{4A_0 A_m}e^{-ik_l L}\right]^{-1}\mathbf{a}^+ \tag{C.13}$$

where subscripts A and B are used to denote the model A and the model B. If the exponential term in the brackets in equation (C.13) is expanded, then,

$$\mathbf{d}_B^{+} = e^{-ik_l L}\left[\frac{(A_0+A_m)(A_m+A_L)}{4A_0A_m}+\frac{(A_m-A_0)(A_L-A_0)}{4A_0A_m}\{1-ik_lL+\ldots\}\right]^{-1}\mathbf{a}^{+}$$

$$= e^{-ik_l L}\left[\frac{A_0+A_L}{2A_0}-ik_lL\frac{(A_m-A_0)(A_L-A_0)}{4A_0A_m}+\ldots\right]^{-1}\mathbf{a}^{+} \qquad \text{(C.14a, b, c)}$$

$$= e^{-ik_l L}\left[\frac{A_0+A_L}{2A_0}-ik_lL\frac{(2\alpha+\alpha^2)^2}{8(2+2\alpha+\alpha^2)}+\ldots\right]^{-1}\mathbf{a}^{+}$$

It can be seen that, when $k_l L \ll 1$, $\mathbf{d}_B^{+}$ asymptotes to $\mathbf{d}_A^{+}$

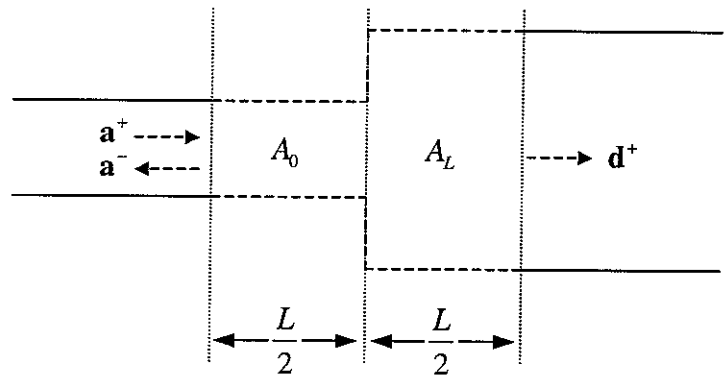

Figure C-2. Discrete model A.

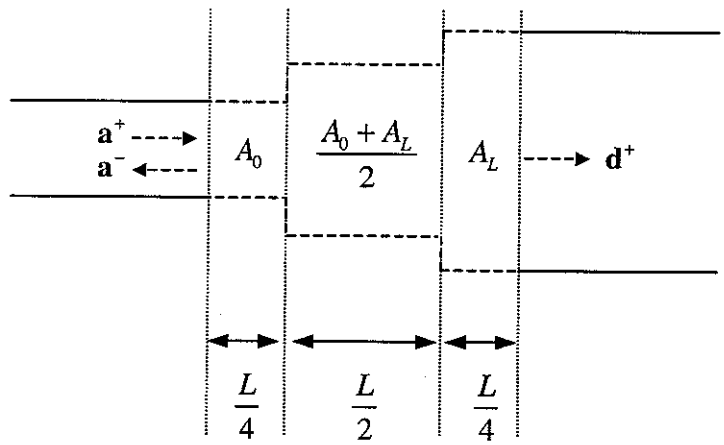

Figure C-3. Discrete model B.

Figure C-4 shows transmissions through the connector obtained by the exact solution and the two discrete models. It can be seen that, when $k_l L \ll 1$, the power transmission coefficients of the three cases all tend to the value given by equation (C.8). Also, it can be

seen that the exact power transmission coefficient tends to unity and the phase of the transmission coefficient tends to zero when $k_t L \gg 1$.

C.3 Error estimation

Figure C-5 shows the errors in the transmission coefficients which occur when the connector is modelled by the discrete models. In the figure, the error, ε_τ, in the power transmission coefficient and the error, ε_θ, in phase of transmission coefficient are given by

$$\varepsilon_\tau = \left| \frac{\tau_e - \tau_d}{\tau_e} \right| \tag{C.15}$$

$$\varepsilon_\theta = \left| \theta_e - \theta_d \right| \tag{C.16}$$

where subscripts e and d denote the exact solution and discrete model, respectively.

In the figure, it can be seen that the higher α becomes, the greater the errors due to the discretization in both models. When $\alpha = 1$, it can also be seen that, if $k_t L \leq \frac{\pi}{10}$, the percentage error in power transmission coefficient obtained by the discrete model A is approximately less than 1% and the error in the phase is less than 0.05 (radian).

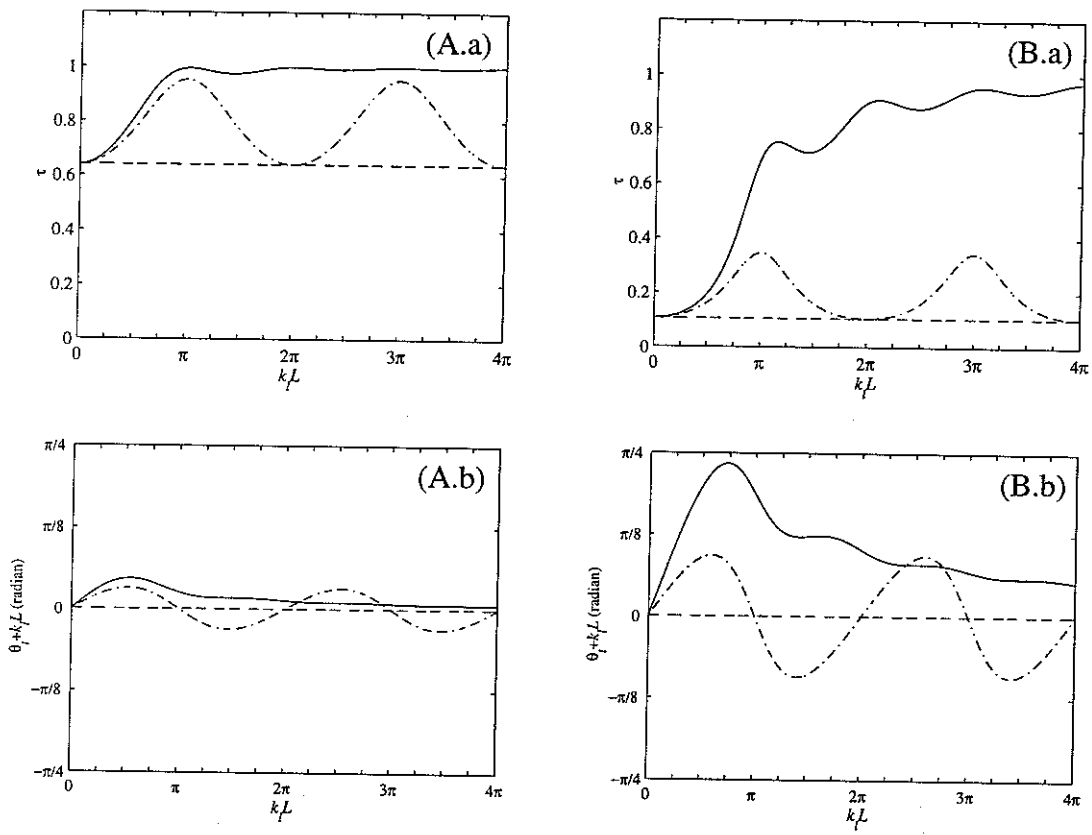

Figure C-4. Transmission through a conical connector: (A) $\alpha = 1$ and (B) $\alpha = 5$; (a) power transmission coefficient and (b) phase of transmission coefficient multiplied by e^{ik_tL}; ——, exact; ------, discrete model A; -·-·-·-, discrete model B.

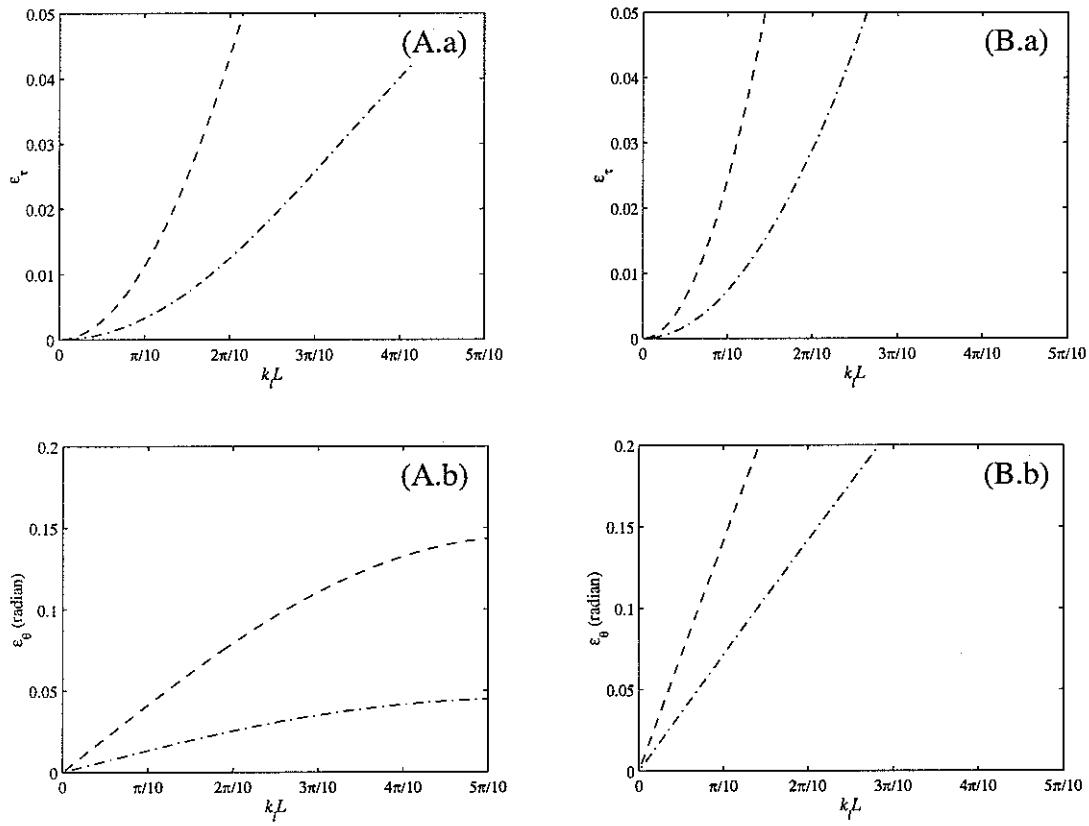

Figure C-5. Errors in predicted transmission through a conical connector due to discretization: (A) $\alpha = 1$ and (B) $\alpha = 5$; (a) error in power transmission coefficient and (b) error in phase of transmission coefficient;

------ , discrete model A; -·-·-·- , discrete model B.

REFERENCES

1. A. D. PIERCE 1981 *Acoustics: An Introduction to Its Physical Principles and Applications*. New York: McGraw-Hill.
2. B. N. NAGARKAR and R. D. FINCH 1971 *Journal of the Acoustical Society of America* **50**, 23-31. Sinusoidal Horns.
3. N. W. McLACHLAN 1955 *Bessel Functions for Engineers (2^{nd} Edition)*. London: Oxford University Press.
4. K.F. GRAFF 1975 *Wave Motion in Elastic Solids*. Oxford: Clarenden Press.
5. B. M. KUMAR and R. I. SUJITH 1997 *Journal of Sound and Vibration* **207**, 721-729. Exact solutions for the longitudinal vibration of non-uniform rods.
6. E. T. CRANCH and A. A. ADLER 1956 *Journal of Applied Mechanics* **23**, 103-108. Bending vibrations of variable section beams.
7. S. ABRATE 1995 *Journal of Sound and Vibration* **185**, 703-716. Vibration of non-uniform rods and beams.
8. E. D. SUPPIGER and N. J. TALEB 1956 *ZAMP* **7**, 501-520. Free lateral vibration of beams of variable cross section.
9. H. C. WANG 1968 *Journal of Applied Mechanics* **34**, 702-708. Generalized hypergeometric function solutions on transverse vibrations of a class of nonuniform beams.
10. H. D. CONWAY, E. C. H. BECKER and J. F. DUBIL 1964 *Transactions of the American Society Mechanical Engineers, Journal of Applied Mechanics* **31**, 329-331. Vibration frequencies of tapered bars and circular plates.
11. H. H. MABIE and C. B. ROGERS 1968 *Journal of the Acoustical Society of America* **44**, 1739-1741. Transverse vibrations of tapered cantilever beams with end support.
12. H. H. MABIE and C. B. ROGERS 1974 *Journal of the Acoustical Society of America* **55**, 986-991. Transverse vibrations of double-tapered cantilever beams with end support and with end mass.
13. R. P. GOEL 1976 *Journal of Sound and Vibration* **47**, 1-7. Transverse vibrations of tapered beams.
14. W. L. CRAVER and P. JAMPALA 1993 *Journal of Sound and Vibration* **166**, 521-529. Transverse vibrations of a linearly tapered cantilever beam with constraining springs.

15. N. M. AUCIELLO and G. NOLE 1998 *Journal of Sound and Vibration* **214**, 105-119. Vibrations of a cantilever tapered beam with varying section properties and carrying a mass at the free end.
16. J. R. BANERJEE and F. W. WILLIAMS 1985 *International Journal for Numerical Methods in Engineering* **21**, 2289-2302. Exact Bernoulli-Euler dynamic stiffness matrix for a range of tapered beams.
17. J. R. BANERJEE and F. W. WILLIAMS 1986 *International Journal for Numerical Methods in Engineering* **23**, 1615-1628. Exact Bernoulli-Euler static stiffness matrix for a range of tapered beam-columns.
18. M. EISENBERGER 1990 *AIAA Journal* **28**, 1105-1109. Exact static and dynamic stiffness matrices for general variable cross section members.
19. D. L. KARABALIS and D. E. BESKOS 1983 *Computers & Structures* **16**, 731-748. Static, dynamic and stability analysis of structures composed of tapered beams.
20. N. M. AUCIELLO 2000 *Journal of Sound and Vibration* **237**, 542-549. Free vibration of a restrained shear-deformable tapered beam with a tip mass at its free end.
21. S. GOPALAKRISHNAN and J. F. DOYLE 1994 *Journal of Sound and Vibration* **175**, 347-363. Wave propagation in connected waveguides of varying cross-section.
22. L. CREMER, M. HECKL and E. E. UNGAR 1973 *Structure-borne Sound.* Berlin: Springer-Verlag.
23. B. R. MACE 1984 *Journal of Sound and Vibration* **97**, 237-246. Wave reflection and transmission in beams.
24. N. R. HARLAND, B. R. MACE and R. W. JONES 2001 *Journal of Sound and Vibration* **241**, 735-754. Wave propagation, reflection and transmission in tunable fluid-filled beams.
25. S-K. LEE, B. R. MACE and M. J. BRENNAN 2003 *ISVR Technical Memorandum* **918** Vibrational Analysis of a Non-Uniform One-Dimensional Structure Using a Wave Approach.
26. M. R. SPIEGEL 1968 *Mathematical Handbook of Formulas and Tables.* Schaum's Outline Series, McGraw-Hill.
27. M. ABRAMOWITZ and I. A. STEGUN 1965 *Handbook of Mathematical Functions with Formulas, Graphs, and Mathematical Tables.* New York: Dover Publications.
28. R. L. FINNEY and D. R. OSTBERG 1976 *Elementary Differential Equations with Linear Algebra.* Addison-Wesley.
29. J. F. DOYLE 1997 *Wave Propagation in Structures: Spectral Analysis using Fast*

Discrete Fourier Transforms. New York: Springer-Verlag.

30. M. J. LIGHTHILL 1978 *Waves in Fluids*. Cambridge: Cambridge University Press.